

MASTER

Galloping transmission lines

Kaisara, T.

Award date:
2008

[Link to publication](#)

Disclaimer

This document contains a student thesis (bachelor's or master's), as authored by a student at Eindhoven University of Technology. Student theses are made available in the TU/e repository upon obtaining the required degree. The grade received is not published on the document as presented in the repository. The required complexity or quality of research of student theses may vary by program, and the required minimum study period may vary in duration.

General rights

Copyright and moral rights for the publications made accessible in the public portal are retained by the authors and/or other copyright owners and it is a condition of accessing publications that users recognise and abide by the legal requirements associated with these rights.

- Users may download and print one copy of any publication from the public portal for the purpose of private study or research.
- You may not further distribute the material or use it for any profit-making activity or commercial gain

TECHNISCHE UNIVERSITEIT EINDHOVEN
Department of Mathematics and Computer Science

Galloping Transmission Lines

by Tefa Kaisara

Supervisor:
Dr. Ir. J.H.M ten Thije Boonkamp

Eindhoven, February 2008

Contents

List of Tables	iii
List of Figures	iii
Abstract	iv
Abstract	v
Acknowledgements	vi
Abstract	vi
1 Introduction	1
2 Problem Formulation	3
2.1 Mathematical model	3
2.2 Reduced problem	6
2.3 Boundary and coupling conditions	8
3 Numerical Solution Procedure	11
3.1 Stationary solution	11
3.2 Non-stationary solution	13

4 Numerical Solution of the Hyperbolic System	16
4.1 Analytical solution	16
4.2 Upwind scheme	17
4.3 ADER schemes	20
4.3.1 ADER scheme for a linear system	23
4.3.2 Reconstruction and initial data	25
4.3.3 Stability analysis	30
4.4 Numerical boundary conditions	30
5 Numerical Results	35
5.1 Numerical experiments for ADER scheme	35
5.2 Cable simulation results	39
6 Conclusion and Recommendations	47
Bibliography	48

List of Tables

5.1	Reconstruction using the fixed stencil approximation of order $m = 2$ and left shift $r = 0$	36
5.2	Reconstruction using the fixed stencil approximation of order $m = 2$ and left shift $r = 1$	36
5.3	Reconstruction using the fixed stencil approximation of order $m = 3$ and left shift $r = 0$	37
5.4	Reconstruction using the fixed stencil approximation of order $m = 3$ and left shift $r = 1$	37
5.5	Reconstruction using the fixed stencil approximation of order $m = 3$ and left shift $r = 2$	38
5.6	Reconstruction using the ENO of order $m = 2$	38
5.7	Reconstruction using the ENO of order $m = 3$	39
5.8	L_2 and L_∞ errors and orders for different Δs , $\gamma = 0.8$ and $t_{max} = 2$	39

List of Figures

2.1	Impression of a suspended cable consisting of two interconnected spans	4
2.2	Tension vector	5
2.3	Sketch of cables connected at a suspension string	9
4.1	Stencil for the upwind scheme	19
4.2	Boundary and coupling conditions of the hyperbolic system . .	31
5.1	An oscillating cable section, for $N_s=100$ and has minimum at $D = 9m$ in both spans,the steady state solution.	41
5.2	An oscillating cable section, for $N_s=100$ and has a minimum= at $8m$	42
5.3	An oscillating cable section, for $N_s=100$ and initially has a minimum at $6m$ in both spans.	43
5.4	An oscillating cable section, for $N_s=100$ and has a minimum at $15m$ in both spans.	44
5.5	An oscillating cable section, for $N_s=100$ and has minimum at $9m$ in the first span and 0 in the second span.	45

Abstract

In this thesis, galloping of overhead transmission lines is studied. This is a low frequency, large amplitude, wind-induced vibrations of both a single and a bundle of overhead transmission lines. The model for this phenomenon is derived from the first principles of Newton's and Hooke's laws.

We analyze the model and develop an algorithm for solving the system. We will present two numerical schemes, that have been chosen for this task, namely the upwind and ADER schemes. Lastly, conduct several galloping simulations under practically relevant conditions.

Acknowledgements

I would like to acknowledge the following people, for without them this study would not have been completed.

- Dr.Ir. J.H.M. ten Thijs Boonkamp, for supervising this project. I thank him very much for his support, patience and guidance.
- My friends and colleagues, Cloo, Vryan, Maxim, Henry, Charles, Patricio, Marnah, Wanda, Yixin, Eric and Robert. For their support, sharing knowledge and the fun we had together.
- My family, for their love, support, prayers also believing in me.
- The staff of both Eindhoven University of Technology and Johannes Kepler University, for their much appreciated assistance for my stay in these two Universities.
- Last but not least, i would like to acknowledge the European Union under the Erasmus Mundus, for their financial support and also for a giving me a chance to study in Europe.

Chapter 1

Introduction

Overhead transmission lines provide the transport highways to move electricity from the generation sources to concentrated areas of customers. From there, the distribution system moves the electricity to where the customer uses it at a business or at home. Unlike other commodities, electricity is generated as it is used and there is very little ability to store it [8]. Because of the instantaneous nature of the electric system, constant modifications must be made to assure that the generation of power matches the consumption of power. The amount of power on a transmission line at any given moment depends on production and dispatch, customer use, the status of other transmission lines and their associated equipment, and even the weather. These transmission lines are cables of aluminium alloy suspended by several towers in a row. The part of the transmission line between two towers is called a span. The cables are connected to the towers by a freely moveable suspension string or insulator, therefore the dynamical motion of neighbouring spans is coupled.

Companies that supply electricity need to defend against weather-related damage and power outages. Ice and snow build-up on high-voltage electric power lines in moderate to high winds cause large scale mechanical vibrations. This phenomenon of low frequency, large amplitude, wind-induced vibrations of both a single and a bundle of overhead transmission lines, with a single or a few standing waves per span, is called *galloping* [3]. Galloping of transmission lines is a dangerous phenomenon that seriously threatens the security of power systems. It is known that galloping causes such serious transmission problems as short circuits due to the entanglement of lines, snapping of the line-to-line spacers and the breakage of transmission towers. It is a result

of aerodynamic instability of conductors related to many aspects, such as parameters of transmission lines, temperature, speed and direction of wind, shape and position of the attached ice, etc [5]. It has attracted the attention of many researchers who are attempting to understand and control this costly vibration. To avoid accidents such as marginal discharge, break or line mixing in regions where galloping is likely to occur, the maximum amplitude of the transmission lines should be calculated. Some analytical and experimental methods have been proposed and implemented in the past years. In general, galloping can roughly be divided into two types, vertical galloping without twist and torsional galloping with elliptical vibrating trajectory [5]. The latter is a much more complex non-linear problem, related to many aerodynamic conditions as well as the stiffness of the conductors.

In this thesis we will consider the former. Although both torsional motion and horizontal cable deflection are important for the full problem we assume torsion to be decoupled from the vertical vibration and the horizontal motion to be negligible. This type of galloping have been mathematically simulated using the finite element method [5], but we will derive a suitable algorithm and numerical techniques (ADER and upwind) for the simulation.

The outline of this thesis is as follows.

In Chapter 2, a mathematical model based on first principles of Newton's and Hooke's law is derived. Asymptotic reduction of the full model, resulting in a systematic model, is discussed [4].

Chapter 3, we come up with a numerical solution procedure by analyzing both the stationary and time dependent part of the systematic model derived in the previous chapter. The procedure includes a hyperbolic system which needs to be solved.

In chapter 4, we discuss the solution of the hyperbolic system. The upwind and ADER schemes are discussed in detail. The abbreviation ADER stands for "Arbitrary high order schemes using DERivatives". This is a finite volume scheme. In general, we approximate every smooth function to arbitrary high order of accuracy using its Taylor expansion. Boundary conditions are also derived.

In chapter 5, the schemes are implemented. Simulations are conducted using practical relevant example parameters from [4]. Numerical results are given.

The last chapter, we summarize the work done, give some conclusive remarks and some ideas for the extension of this work.

Chapter 2

Problem Formulation

In this chapter we will derive a systematic model by asymptotic reduction of the model found in [4] and [3]; details on asymptotic reduction are found in the same references. We derive the model from the first principles of Newton's and Hooke's laws. Then present a reduced model based on asymptotic analysis. Last in this chapter we shall discuss boundary and coupling conditions.

2.1 Mathematical model

We consider a cable fixed at the outer ends, and divided into N equal spans by $N - 1$ equal supports. The supports are inextensible suspension strings (isolators) of length a and negligible weight, suspended from fixed pivots separated by a distance $S(m)$, the span size. We assume that the cable is linearly elastic, with negligible bending stiffness, of uniform undeformed effective cross section $A(m^2)$, mass per unit length $m(kg/m)$, and Young's modulus $E(N/m^2)$. We define the length per span when the cable is free of tension to be $L(m)$. If stationary, each span has the maximum deflection, the so-called sag $D(m)$, which depends on S and L , see Figure 2.1.

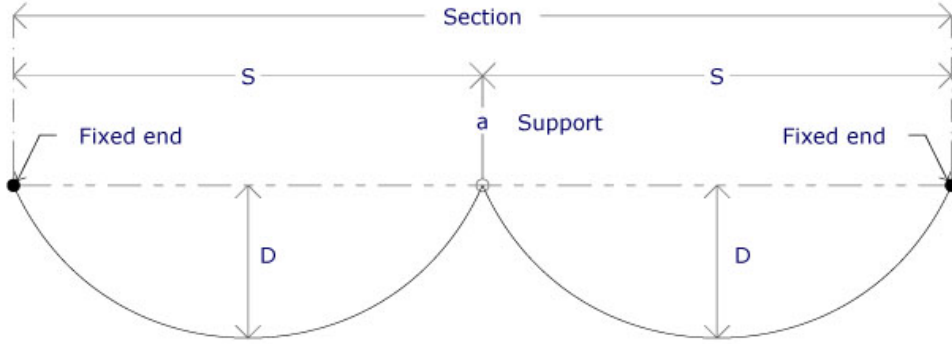


Figure 2.1: Impression of a suspended cable consisting of two interconnected spans

Let $\ell \in [0, NL]$, describe the position along the cable such that it represents the arc length when the cable is unstretched, i.e., there is no tension in the cable. The dimensional time variable is denoted by t . Although in reality the cable moves along a slightly tilted ellipse, we will consider only the cable motion in a vertical plane which is provided with a Cartesian coordinate system orientated such that the gravity vector $-g\mathbf{e}_y$ points into the negative y -direction. The cable position is defined by the position vector $\mathbf{X}(\ell, t) = (X(\ell, t), Y(\ell, t))$, measured in meters, with a corresponding tension vector $\mathbf{T}(\ell, t) = T(\ell, t)(\cos \psi, \sin \psi)$, measured in Newtons, where ψ is the positively oriented angle between the cable tangent and the horizontal. The tension vector is tangent to the cable because of the assumed negligible bending stiffness; see Figure 2.2.

Let us now consider a small cable element $d\ell$. The element is stretched due to gravity, cable tension and inertial forces but we note that the mass does not change. According to Hooke's law [9], which states that the amount by which a material body is deformed (the strain) is linearly proportional to the force causing the deformation (the stress), a cable element is elongated in proportional to the tension and can therefore be represented by

$$\frac{\sqrt{(dX)^2 + (dY)^2} - d\ell}{d\ell} = \frac{1}{E} \frac{T}{A}. \quad (2.1)$$

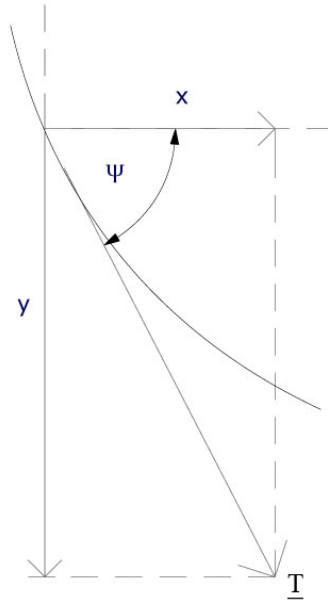


Figure 2.2: Tension vector

Rearranging terms in equation (2.1), we obtain

$$\left(\frac{\partial X}{\partial \ell}\right)^2 + \left(\frac{\partial Y}{\partial \ell}\right)^2 = \left(1 + \frac{T}{EA}\right)^2. \quad (2.2)$$

According to Newton's second law, the net force on a particle is proportional to the rate of its linear momentum, usually represented as $F = ma$. Since momentum is a product of mass and velocity, this is given by

$$\frac{\partial \mathbf{T}}{\partial \ell} = m \left(\frac{\partial^2 \mathbf{X}}{\partial t^2} + g \mathbf{e}_y \right). \quad (2.3)$$

The x -component of the tension is given by

$$\frac{\partial}{\partial \ell}(T_x) = m \frac{\partial^2 X}{\partial t^2}, \quad (2.4)$$

and along the y -component, since gravitational force is acting, the tension is described by

$$\frac{\partial}{\partial \ell}(T_y) = m \left(\frac{\partial^2 X}{\partial t^2} + g \right), \quad (2.5)$$

where $T_x = T \cos \psi$ and $T_y = T \sin \psi$. The tension vector is tangent to the cable because of the assumed negligible bending stiffness. From (2.2) it is obvious that

$$\left| \frac{\partial \mathbf{X}}{\partial \ell} \right| = 1 + \frac{T}{EA}, \quad (2.6)$$

and therefore we have the sine and cosine of ψ defined by

$$\cos \psi = \frac{\frac{\partial X}{\partial \ell}}{1 + \frac{T}{EA}}, \quad \sin \psi = \frac{\frac{\partial Y}{\partial \ell}}{1 + \frac{T}{EA}}. \quad (2.7)$$

We then substitute (2.7) into (2.4) and (2.5) resulting in the system

$$\frac{\partial}{\partial \ell} \left(\frac{T}{1 + T/EA} \frac{\partial X}{\partial \ell} \right) = m \frac{\partial^2 X}{\partial t^2}, \quad (2.8a)$$

$$\frac{\partial}{\partial \ell} \left(\frac{T}{1 + T/EA} \frac{\partial Y}{\partial \ell} \right) = m \frac{\partial^2 Y}{\partial t^2} + mg. \quad (2.8b)$$

The mathematical model is described by (2.2) and (2.8).

2.2 Reduced problem

The type of motion we are interested in allows further reduction of the model. This is motivated by the ratio of sag D , which is the stationary vertical displacement and the cable length L . The ratio is known to be small, according to [3] it is typically in the order of $\frac{1}{30}$. Therefore we have the slenderness,

$$\varepsilon = D/L \rightarrow 0$$

and this is clearly a small parameter problem. This basic small parameter ε is used to reduce the general problem to an asymptotic model. Asymptotic

methods are usually most powerful precisely when numerical approaches encounter their most serious difficulties, such as in cases of small parameters, phenomena on vastly different scales etc. Perturbation / asymptotic analysis can then provide accurate information in analytic forms which are very well suited for both understanding and for further analysis [6].

The longitudinal wave speed is given by $c_L = (EA/m)^{\frac{1}{2}}$, and the longitudinal wave length λ_L is large compared to the length of the cable L leading to the estimate $L/\lambda_L = \mathcal{O}(\varepsilon)$. The frequency ω is inversely proportional to the wave length and we have $L/\lambda_L = \omega L/c_L = \mathcal{O}(\varepsilon)$. We now introduce the reference frequency $\omega_{ref} = \varepsilon c_L/L$. The dimensionless frequency ω^* and time variable t^* are given by

$$\omega = \omega_{ref}\omega^*, \quad t = t^*/\omega_{ref}. \quad (2.9)$$

We also have that the total vertical non-stationary displacement Y is of the order of the sag D , and the transversal wave length λ_T is of order L so that $Y/L = \mathcal{O}(\varepsilon)$ and $\lambda_T/L = \mathcal{O}(1)$. Clearly, we see that Y scales on εL . The transversal wave velocity is given by $c_T = (T/m)^{\frac{1}{2}}$, thus we have $\lambda_T/L = c_T/\omega L = \mathcal{O}(1)$. This yields that the tension scales on $T_{ref} = \varepsilon^2 EA$. Putting everything together, we have for $\ell \in \{\text{the } n\text{-th span}\}$

$$\ell = (n-1+s)L, \quad Y(\ell, t) = \varepsilon LY^*(s, t^*; n), \quad T(\ell, t) = T_{ref} T^*(s, t^*; n), \quad (2.10)$$

where (*) are dimensionless variables and where the variable s is a local nondimensional parameter, such that $s \in [0, 1]$ parametrizing the position within a span. We also have to scale X , and we are only interested in the x -displacements that are very small. By substituting the above estimates in equation (2.8b), it transpires that $\frac{\partial}{\partial \ell} X = 1 + \mathcal{O}(\varepsilon^2)$, therefore for X from the n -th span we have

$$X(\ell, t) = (n-1)S + Ls + \varepsilon^2 LX^*(s, t^*; n). \quad (2.11)$$

If we substitute the present estimates in (2.8b), we get the term $mgL/EA\varepsilon^3$ next to terms of order 1, so it is either has to be of order 1 or smaller. Assuming that it is smaller, then the stationary solution would be $Y = 0$ to leading order, so $D = 0$, which contradicts our scaling assumptions. Therefore it follows that the term is of order 1. We introduce

$$\mu = \frac{mgL}{8EA\varepsilon^3} = \mathcal{O}(1) \quad (2.12)$$

where the factor 8 comes from the assumption that the cable has a ratio of sag to span of about 1:8 see [7]. For details on asymptotic expansions see [4] and [3].

Finally, we substitute all the above estimates in the system of equations (2.2) and (2.8). We obtain, under the approximation of small ε , the governing equations [4].

$$\frac{\partial T^*}{\partial s} = 0, \quad (2.13a)$$

$$\frac{\partial}{\partial s} \left(T^* \frac{\partial Y^*}{\partial s} \right) = 8\mu + \frac{\partial^2 Y^*}{\partial t^{*2}}, \quad (2.13b)$$

$$\frac{\partial X^*}{\partial s} + \frac{1}{2} \left(\frac{\partial Y^*}{\partial s} \right)^2 = T^*. \quad (2.13c)$$

2.3 Boundary and coupling conditions

In this section we derive the boundary and coupling conditions for the model of two spans ($N = 2$). We will then scale them using the estimates from the previous section.

- We have fixed supports at $\ell = 0$ and $\ell = 2L$, therefore we have

$$X(0, t) = 0, \quad Y(0, t) = 0 \quad (\ell = 0), \quad (2.14a)$$

$$X(2L, t) = 2S \quad Y(2L, t) = 0 \quad (\ell = 2L). \quad (2.14b)$$

- At the suspension string $\ell = L$ the position vector \mathbf{X} is continuous, the rigid but hinged suspension strings restrict the motion to a circle, while the force component normal to the string is continuous [3]. This gives the coupling conditions

$$\mathbf{X}(L+, t) - \mathbf{X}(L-, t) = 0 \Leftrightarrow \begin{cases} X(L+, t) = X(L-, t) \\ Y(L+, t) = Y(L-, t) \end{cases} \quad (2.15a)$$

$$(X - S)^2 + (Y - a)^2 = a^2, \quad (2.15b)$$

$$[T \cos(\phi - \psi)]_{\ell=L-}^{\ell=L+} = 0, \quad (2.15c)$$

where ϕ denotes the positively oriented angle of the suspension string with the vertical and $\ell = L\pm$ denotes the limit from either side of the support, see Figure 2.3.

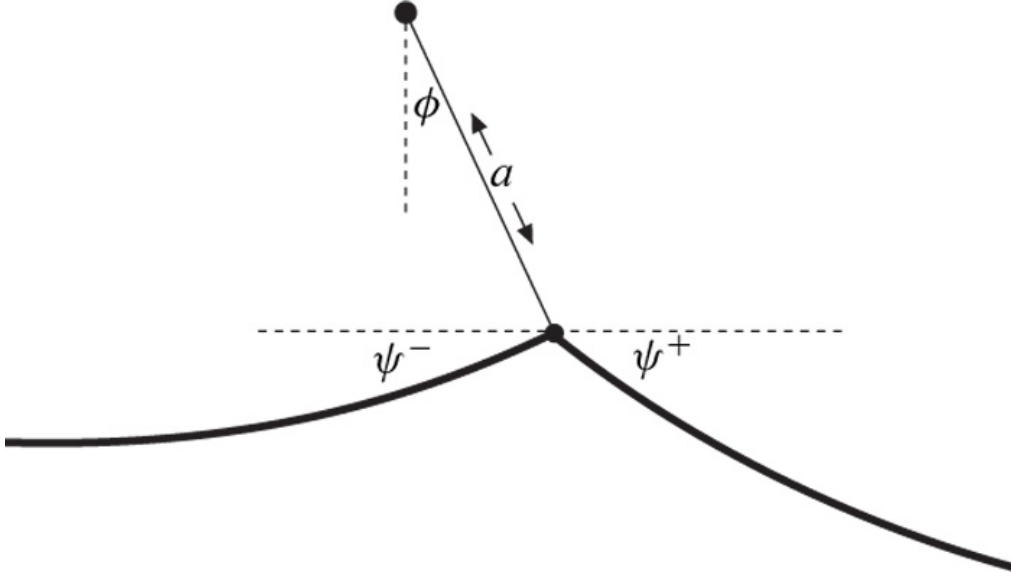


Figure 2.3: Sketch of cables connected at a suspension string

In the first span we have $n = 1$ and $s \in [0, 1]$. Substituting these into the relations (2.10) and (2.11) we have

$$\begin{aligned} \ell = sL, \quad Y(\ell, t) = \varepsilon LY^*(s, t^*; 1), \quad T(\ell, t) = T_{ref} T^*(s, t^*; 1), \\ X(\ell, t) = Ls + \varepsilon^2 LX^*(s, t^*; 1). \end{aligned} \quad (2.16)$$

At the first fixed support we have $s = 0$ and $\ell = 0$, hence we obtain the boundary conditions

$$X(0, t) = 0 \iff \varepsilon^2 LX^*(0, t^*; 1) = 0 \iff X^*(0, t^*; 1) = 0, \quad (2.17)$$

$$Y(0, t) = 0 \iff \varepsilon LY^*(0, t^*; 1) = 0 \iff Y^*(0, t^*; 1) = 0. \quad (2.18)$$

For the second span we have $n = 2$ and $s \in [0, 1]$ and substituting these into (2.10) and (2.11) we have

$$\begin{aligned} \ell = (1 + s)L, \quad Y(\ell, t) = \varepsilon LY^*(s, t^*; 2), \quad T(\ell, t) = T_{ref} T^*(s, t^*; 2), \\ X(\ell, t) = S + Ls + \varepsilon^2 LX^*(s, t^*; 2). \end{aligned} \quad (2.19)$$

In the second span there is a fixed support at the end point, where $\ell = 2L$ and $s = 1$, leading to the boundary conditions

$$\begin{aligned} X(2L, t) = 2S &\iff S + L + \varepsilon^2 LX^*(1, t^*; 2) = 2S \\ &\iff X^*(1, t^*; 2) = \frac{S - L}{\varepsilon^2 L} = S_0, \\ Y(2L, t) = 0 &\iff \varepsilon LY^*(1, t^*; 2) = 0 \iff Y^*(1, t^*; 2) = 0. \end{aligned} \quad (2.20)$$

For the conditions at the suspension string we have for the first span, $s = 1$ and $\ell = 1$ and for the same point on the second span we have $s = 0$ and $\ell = 2$. It is observed that $a\phi/L = \mathcal{O}(\varepsilon^2)$, as it is of order of the x -variation, therefore $\phi = \mathcal{O}(\varepsilon)$ [3]. For small ε we obtain the scaled coupling conditions.

From (2.15c) we have

$$T^*(1, t^*; 1) = T^*(0, t^*; 2). \quad (2.21)$$

We have

$$\begin{aligned} Y(L, t) = 0 &\iff \varepsilon LY^*(1, t^*; 1) = \varepsilon LY^*(0, t^*; 2) = 0 \\ &\iff Y^*(1, t^*; 1) = Y^*(0, t; 2) = 0. \end{aligned} \quad (2.22)$$

For $X(L, t)$ we have the coupling condition

$$\begin{aligned} X(L-, t) = X(L+, t) &\iff L + \varepsilon^2 LX^*(1, t^*; 1) = S + \varepsilon^2 LX^*(0, t^*; 2) = 0 \\ &\iff X^*(1, t^*; 1) = X^*(0, t^*; 2) + S_0. \end{aligned} \quad (2.23)$$

Chapter 3

Numerical Solution Procedure

In this chapter we will analyze how to solve the governing equations (2.13) incorporating the boundary and the coupling conditions derived in the previous chapter. In practice, the sag D and the span size S are known but the length of the cable L is unknown and is to be determined. This means that ε and μ are to be determined from the stationary solution. We assume that all problem parameters are the same for all spans and hence the stationary solution is periodic in space. This motivates the analysis of a stationary and a nonstationary part. The stationary solution will later be used as the initial condition for the nonstationary solution.

3.1 Stationary solution

For the steady part of the problem we will represent the variables with a subscript 0, and then from (2.10) and (2.11) we have

$$\begin{aligned} T_0(\ell) &= T_{ref} \cdot T_0^*(s; n), & X_0(\ell) &= (n-1)S + Ls + \varepsilon^2 L X_0^*(s; n), \\ & & Y_0(\ell) &= \varepsilon L Y_0^*(s; n). \end{aligned} \quad (3.1)$$

We then have the governing equations for the stationary state given by

$$\frac{dT_0^*}{ds} = 0, \quad (3.2a)$$

$$T_0^* \frac{d^2 Y_0^*}{ds^2} = 8\mu, \quad (3.2b)$$

$$\frac{dX_0^*}{ds} + \frac{1}{2} \left(\frac{dY_0^*}{ds} \right)^2 = T_0^*. \quad (3.2c)$$

For the first span we have the boundary conditions, $Y_0^*(0; 1) = Y_0^*(1; 1) = 0$ and $X_0^*(0; 1) = 0$. Since Y is scaled on the sag D , from symmetry we expect the location of the maximum deflection half-way, hence we have $Y(\frac{1}{2}L) = -D \Leftrightarrow Y_0^*(\frac{1}{2}; 1) = -1$. To compute Y_0^* we integrate twice equation (3.2b) on the interval $[0, 1]$ with respect to s and incorporate the boundary equations. To find the steady solution of \mathbf{T} we substitute the maximum deflection condition of Y_0^* . We obtain

$$T_0^*(s; 1) = \mu \quad \text{and} \quad Y_0^*(s; 1) = 4s(s - 1). \quad (3.3)$$

We note that at the suspension spring, $s = 1$, we do not have a boundary but a coupling condition which implicitly determines the unknown length L . Therefore, substituting Y_0^* into (3.2c), integrate the equation with respect to s and incorporate the boundary condition we obtain

$$X_0^*(s; 1) = \mu s - \frac{4}{3}[(2s - 1)^3 + 1]. \quad (3.4)$$

The distance from the first fixed point to the suspension point is just the span size S , thus we have

$$X_0^*(L) = S \iff L + \varepsilon^2 L X_0^*(1; 1) = S. \quad (3.5)$$

Since from (3.4) we have $X_0^*(1; 1) = \mu - \frac{8}{3}$, we now have

$$X_0^*(L) = S_0 \iff L^2 - SL + D^2 \left(\mu - \frac{8}{3} \right) = 0, \quad D = \varepsilon L. \quad (3.6)$$

Substituting $\mu = \frac{mgL}{8EA\varepsilon^3}$ in (3.6) we obtain the equation which determines the length L , i.e.,

$$\alpha L^4 + L^2 - SL - \frac{8}{3}D^2 = 0 \quad \alpha := \frac{mg}{8EAD}. \quad (3.7)$$

In the second span we have $\ell = (1 + s)L$. For the boundaries we have the first suspension string $s = 0$, $\ell = L$ and the condition $Y_0(L) = 0 \Leftrightarrow Y_0^*(0; 2) = 0$. At the last fixed support $s = 1$, $\ell = 2L$ we have the boundary condition $Y_0(2L) = 0 \Leftrightarrow Y_0^*(1; 2) = 0$. From symmetry we assume again

that the maximum deflection is halfway the second span, hence we have $Y(\frac{3}{2}L) = -D \Leftrightarrow Y_0^*(\frac{1}{2}; 2) = -1$. We obtain the solutions for the second span

$$T_0^*(s; 2) = \mu, \quad Y_0^*(s; 2) = 4s(s-1), \quad X_0^*(s; 2) = \mu s - \frac{4}{3}[(2s-1)^3 + 1]. \quad (3.8)$$

These results show that the solution is indeed periodic and we have the last boundary condition automatically satisfied, i.e.,

$$X_0^*(2L) = 2S_0 \iff X_0^*(L) = S_0. \quad (3.9)$$

3.2 Non-stationary solution

In this section we will analyze the solution of the time depend part of the governing equations. From (2.13a) we have $T^* = T^*(t^*)$ in a single span. Since we have the coupling condition (2.21) we conclude that

$$T^*(t^*; 1) = T^*(t^*; 2) = T^*(t^*). \quad (3.10)$$

From (2.13b) we have

$$T^* \frac{\partial^2 Y^*}{\partial s^2} = \frac{\partial^2 Y^*}{\partial t^2} + 8\mu. \quad (3.11)$$

We define

$$v := \frac{\partial Y^*}{\partial t} + 8\mu t, \quad w := \frac{\partial Y^*}{\partial s}. \quad (3.12)$$

We then obtain

$$\frac{\partial v}{\partial t^*} = \frac{\partial^2 Y^*}{\partial t^{*2}} + 8\mu = T^* \frac{\partial^2 Y^*}{\partial s^{*2}} = T^* \frac{\partial w}{\partial s} \quad (3.13a)$$

$$\frac{\partial w}{\partial t^*} = \frac{\partial}{\partial s} \left(\frac{\partial Y^*}{\partial t^*} \right) = \frac{\partial}{\partial s} (v - 8\mu t^*) = \frac{\partial v}{\partial s}. \quad (3.13b)$$

Substituting w into equation (2.13c) we obtain

$$\frac{\partial X^*}{\partial s} + \frac{1}{2}w^2 = T^*. \quad (3.14)$$

From (3.13) we have

$$\frac{\partial \mathbf{u}}{\partial t} + \mathbf{A} \cdot \frac{\partial \mathbf{u}}{\partial s} = 0, \quad (3.15)$$

where

$$\mathbf{u} = \begin{pmatrix} v \\ w \end{pmatrix} \quad \mathbf{A}(\mathbf{u}) = \begin{pmatrix} 0 & -T^* \\ -1 & 0 \end{pmatrix}.$$

Note that since $T^* = T^*(t^*)$, we have $A = A(t^*)$. The matrix A has two different nonzero eigenvalues and two linearly independent eigenvectors. It then follows that system (3.15) is diagonalizable and therefore hyperbolic. Numerical methods used to solve this hyperbolic system will be discussed in detail in the next chapter. $Y^*(s, t^*; n)$ can therefore be computed per span from the solutions w or v by integrating with respect to s equation $w = \frac{\partial Y^*}{\partial s}$. From (3.14) we can compute the tension. Integrating equation (3.14) with respect to s over the first span and incorporating the boundary condition $X^*(0, t^*; 1) = 0$ we obtain

$$T^*(t^*) = X^*(1, t^*; 1) + \frac{1}{2} \int_0^1 w^2(s, t^*; 1) ds > 0. \quad (3.16)$$

For the second span we apply the same procedure but use the boundary condition $X^*(1, t^*; 2) = S_0$ and we obtain

$$T^*(t^*) = S_0 - X^*(0, t^*; 2) + \frac{1}{2} \int_0^1 w^2(s, t^*; 2) ds. \quad (3.17)$$

To find the tension in both spans we add the two relations (3.16), (3.17) and apply the coupling condition $X^*(1, t^*; 1) - X^*(0, t^*; 2) = S_0$ and obtain the expression

$$T^*(t^*) = S_0 + \frac{1}{4} \int_0^1 w^2(s, t^*; 1) ds + \frac{1}{4} \int_0^1 w^2(s, t^*; 2) ds. \quad (3.18)$$

We then compute $X^*(s, t^*; n)$. We differentiate (3.14) with respect to s and obtain

$$\frac{\partial^2 X^*}{\partial s^2} + w \frac{\partial w}{\partial s} = 0. \quad (3.19)$$

We solve this system per span and incorporate the boundary conditions $X^*(0, t^*; 1) = 0, X^*(1, t^*; 2) = S_0$ and the coupling condition $X^*(1, t^*; 1) = S_0 + X^*(0, t^*; 2)$.

We summarize the procedure discussed above in the form of an algorithm

Algorithm 1 Swinging cables algorithm

- 1: Compute L from $\alpha L^4 + L^2 - SL - \frac{8}{3}D^2 = 0$, $\alpha := \frac{mg}{8EAD}$
 compute $\varepsilon = \frac{D}{L}$, $\mu = \frac{\alpha L^4}{D^2}$, $S_0 = \mu - \frac{8}{3}$
 - 2: Give initial conditions: $X_0^*(s)$, $Y_0^*(s)$, T_0^*
 - 3: Compute $T^*(0)$
 $T^*(0) = S_0 + \frac{1}{4} \int_0^1 w^2(s, 0; 1) ds + \frac{1}{4} \int_0^1 w^2(s, 0; 2) ds$
 - 4: **repeat**
 - 5: Solve $\frac{\partial \mathbf{u}_n}{\partial t^*} + A \cdot \frac{\partial \mathbf{u}_n}{\partial s} = 0$ (numerical scheme)
 - 6: Compute $Y^*(s, t^*; n)$.
 $\frac{\partial Y_n^*}{\partial s} = w_n$
 $Y^*(0, t^*; 1) = 0$, $Y^*(1, t^*; 1) = 0$
 $Y^*(0, t^*; 2) = 0$, $Y^*(1, t^*; 2) = 0$.
 - 7: Compute $T^*(t^*)$
 $T^*(t^*) = S_0 + \frac{1}{4} \int_0^1 w^2(s, t^*; 1) ds + \frac{1}{4} \int_0^1 w^2(s, t^*; 2) ds$
 - 8: Solve $\frac{\partial^2 X_n^*}{\partial s^2} + w_n \cdot \frac{\partial w_n}{\partial s} = 0$
 $X^*(0, t^*; 1) = 0$, $X^*(1, t^*; 2) = S_0$
 $X^*(1, t^*; 1) = S_0 + X^*(0, t^*; 2)$.
 - 9: $t^{*n} = t^{*n+1}$
 - 10: **until** t_{max}
-

Chapter 4

Numerical Solution of the Hyperbolic System

In this chapter we present two numerical schemes, viz the upwind and the ADER schemes, to solve the linear system of hyperbolic conservation laws. First we will compute the analytical solution of system (3.15). We will then derive the two numerical schemes and apply the schemes to our problem of interest. Stability for both schemes is investigated. Finally we derive boundary conditions.

4.1 Analytical solution

Considering the initial value problem

$$\mathbf{u}_t + A\mathbf{u}_s = 0 \quad \text{in } \mathbb{R}^2 \times (0, T_{\max}), \quad (4.1a)$$

$$\mathbf{u}(s, 0) = \mathbf{v}(s) \quad \text{in } \mathbb{R}^2, \quad (4.1b)$$

where

$$\mathbf{u} = \begin{pmatrix} v \\ w \end{pmatrix} \quad \mathbf{A} = \begin{pmatrix} 0 & -T^* \\ -1 & 0 \end{pmatrix}.$$

The matrix \mathbf{A} has the eigensystem,

$$\mathbf{r}_1 = \begin{pmatrix} c \\ 1 \end{pmatrix}, \quad \mathbf{r}_2 = \begin{pmatrix} -c \\ 1 \end{pmatrix}, \quad \lambda_1 = -c < 0, \quad \lambda_2 = c > 0, \quad c = \sqrt{T^*}. \quad (4.2)$$

Since we have two linear independent eigenvectors, the system (4.1) is diagonalizable so that $\mathbf{A} = \mathbf{R}\Lambda\mathbf{R}^{-1}$ where $\Lambda = \text{diag}(\lambda_1, \lambda_2)$ and $\mathbf{R} = (\mathbf{r}_1 \ \mathbf{r}_2)$. We now introduce the characteristic variable $\tilde{\mathbf{u}}(s, t) := \mathbf{R}^{-1}\mathbf{u}(s, t)$ satisfying the decoupled system

$$\tilde{\mathbf{u}}_t + \Lambda\tilde{\mathbf{u}}_s = 0. \quad (4.3)$$

We have the characteristic variable $\tilde{\mathbf{u}}$ given by $\tilde{\mathbf{u}}(s, t) = \mathbf{R}^{-1}\mathbf{u}(s, t)$ componentwise, we obtain

$$\tilde{v} = \frac{1}{2} \left(\frac{v}{c} + w \right), \quad \tilde{w} = \frac{1}{2} \left(-\frac{v}{c} + w \right). \quad (4.4)$$

We find, see [4], $\tilde{v}(s, t) = \tilde{v}(s + ct, 0)$ and $\tilde{w}(s, t) = \tilde{w}(s - ct, 0)$.

Combining these results with the above relations for the characteristic variables, we obtain the analytic solution,

$$v(s, t) = \frac{1}{2} \left[v_1(s + ct) + v_1(s - ct) + c(v_2(s + ct) - v_2(s - ct)) \right], \quad (4.5a)$$

$$w(s, t) = \frac{1}{2} \left[\frac{1}{c} (v_1(s + ct) - v_1(s - ct)) + (v_2(s + ct) + v_2(s - ct)) \right], \quad (4.5b)$$

thus the solution \mathbf{u} consists of two components, one propagating with velocity $\lambda_1 = -c$ and the other with velocity $\lambda_2 = c$. Since $\lambda_1 < 0$, a wave propagates in the negative x -direction and since $\lambda_2 > 0$, the other wave propagates in the positive x -direction.

4.2 Upwind scheme

In order to compute a numerical solution of (3.15), we cover the domain $\Omega := \mathbb{R} \times [0, \infty)$ with grid point (s_j, t^n) , where $s_j := j\Delta s$ for $j \in \mathbb{Z}$ and $t^n := n\Delta t$ for $n \in \mathbb{N}$ with Δs the spatial grid size and Δt the time step. We will

first introduce the upwind scheme for the componentwise decoupled system and subsequently give the scheme for \mathbf{u} . Since by (4.5) each component of the solution is constant along characteristics and therefore has an upwind direction determined by the sign of the corresponding eigenvalue λ_k . The eigenvalues λ_k are split as

$$\lambda_k = \lambda_k^+ + \lambda_k^-, \quad \lambda_k^+ := \max(\lambda_k, 0) \geq 0, \quad \lambda_k^- := \min(\lambda_k, 0) \leq 0. \quad (4.6)$$

We therefore have the upwind scheme for componentwise decoupled system as follows

$$\frac{1}{\Delta t}(\tilde{u}_{k,j}^{n+1} - \tilde{u}_{k,j}^n) + \frac{\lambda_k^+}{\Delta s}(\tilde{u}_{k,j}^n - \tilde{u}_{k,j-1}^n) + \frac{\lambda_k^-}{\Delta s}(\tilde{u}_{k,j+1}^n - \tilde{u}_{k,j}^n) = 0, \quad (4.7)$$

where $k = 1, 2$. $\tilde{u}_{k,j}^n$ denotes the numerical approximation of $\tilde{u}_k(s_j, t^n)$ and we have $\tilde{u}_{1,k}^n = \tilde{v}_k^n$ while $\tilde{u}_{2,k}^n = \tilde{w}_k^n$. The upwind scheme for all characteristic variables \tilde{u}_k can be combined in vector form and we have

$$\frac{1}{\Delta t}(\tilde{\mathbf{u}}_j^{n+1} - \tilde{\mathbf{u}}_j^n) + \frac{\Lambda^+}{\Delta s}(\tilde{\mathbf{u}}_j^n - \tilde{\mathbf{u}}_{j-1}^n) + \frac{\Lambda^-}{\Delta s}(\tilde{\mathbf{u}}_{j+1}^n - \tilde{\mathbf{u}}_j^n) = \mathbf{0}, \quad (4.8)$$

where, $\Lambda^+ := \text{diag}(\lambda_1^+, \lambda_2^+)$ and $\Lambda^- := \text{diag}(\lambda_1^-, \lambda_2^-)$. To formulate the upwind scheme in terms of the original variable \mathbf{u} we substitute the condition $\tilde{\mathbf{u}} := \mathbf{R}^{-1}\mathbf{u}$ into (4.8) and multiply the resulting scheme by matrix \mathbf{R} giving

$$\frac{1}{\Delta t}(\mathbf{u}_j^{n+1} - \mathbf{u}_j^n) + \frac{\mathbf{A}^+}{\Delta s}(\mathbf{u}_j^n - \mathbf{u}_{j-1}^n) + \frac{\mathbf{A}^-}{\Delta s}(\mathbf{u}_{j+1}^n - \mathbf{u}_j^n) = \mathbf{0}, \quad (4.9)$$

where $\mathbf{A}^+ := \mathbf{R}\Lambda^+\mathbf{R}^{-1}$, $\mathbf{A}^- := \mathbf{R}\Lambda^-\mathbf{R}^{-1}$ and $\mathbf{A} = \mathbf{A}^+ + \mathbf{A}^-$. From (4.1) and (4.2) we have

$$\mathbf{A}^+ = \frac{1}{2} \begin{pmatrix} c & -c^2 \\ -1 & c \end{pmatrix}, \quad \mathbf{A}^- = -\frac{1}{2} \begin{pmatrix} c & c^2 \\ 1 & c \end{pmatrix}.$$

Substituting \mathbf{A}^+ and \mathbf{A}^- into (4.9) we obtain the scheme

$$v_j^{n+1} = v_j^n + \frac{1}{2}\gamma [(v_{j+1}^n - 2v_j^n + v_{j-1}^n) + c(w_{j+1}^n - w_{j-1}^n)], \quad (4.10a)$$

$$w_j^{n+1} = w_j^n + \frac{1}{2}\gamma \left[\frac{1}{c}(v_{j+1}^n - v_{j-1}^n) + (w_{j+1}^n - 2w_j^n + w_{j-1}^n) \right]. \quad (4.10b)$$

where $\gamma = c \frac{\Delta t}{\Delta s}$.

The stability of the upwind scheme is ensured if the corresponding scalar upwind schemes for all variables \tilde{u}_k are stable. This is shown in details in [4]. This requirement gives the Courant, Friedrichs and Lewy (CFL) stability condition

$$\lambda \frac{\Delta t}{\Delta s} \leq 1 \iff c \frac{\Delta t}{\Delta s} \leq 1, \quad (4.11)$$

where λ is the maximum absolute eigenvalue of the problem. This requirement means that all characteristics through the point (s_j, t^{n+1}) intersect the grid line $t = t^n$ at the points in the interval $[s_{j-1}, s_{j+1}]$, see Figure 4.1. Since the stability condition restricts the choice of the time step, the upwind scheme is termed to be conditionally stable.

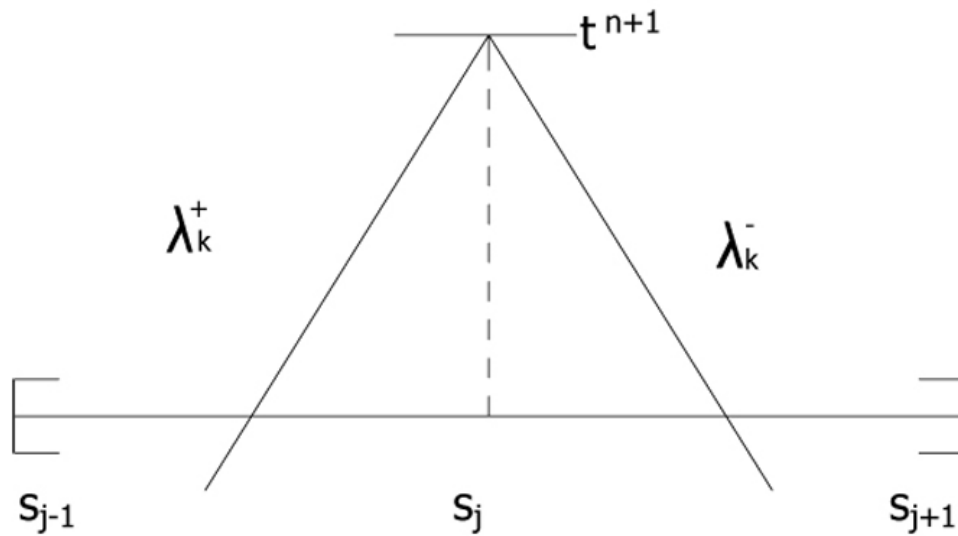


Figure 4.1: Stencil for the upwind scheme

4.3 ADER schemes

ADER is an abbreviation for “Arbitrary high order schemes using DERivatives”. This a finite volume scheme, the hyperbolic conservation laws are integrated over a control-volume which covers space and time. The special feature of the ADER is the computation of the numerical flux. In this section we will derive the ADER scheme by solving the general system of hyperbolic conservation laws. We will introduce the notation needed and the basic principle of the ADER scheme. Finally we will show how the ADER scheme works for our linear hyperbolic system (4.1).

Considering the general system of one-dimensional hyperbolic conservation laws

$$\frac{\partial \mathbf{u}}{\partial t} + \frac{\partial}{\partial s} \mathbf{F}(\mathbf{u}) = \mathbf{0}, \quad s \in \mathbb{R}, t > 0, \quad (4.12)$$

with the initial solution $\mathbf{u}(x, 0) = \mathbf{u}_0(s)$. For the spatial coordinates we use a uniform grid, which contains the cells $I_i = [s_{i-\frac{1}{2}}, s_{i+\frac{1}{2}}]$, for $i \in \mathbb{Z}$ of grid size $\Delta s = s_{i+\frac{1}{2}} - s_{i-\frac{1}{2}}$. Time is also divided uniformly with the time levels denoted by $t^n, n \in \mathbb{N}$ and the stepsize by Δt . Applying the finite volume scheme to (4.12), we integrate over the control volume $V := I_i \times [t^n, t^{n+1}]$ and obtain

$$\mathbf{u}_i^{n+1} = \mathbf{u}_i^n - \frac{\Delta t}{\Delta s} (\mathbf{F}_{i+\frac{1}{2}} - \mathbf{F}_{i-\frac{1}{2}}), \quad (4.13)$$

where the cell average value and the time average flux are given by

$$\mathbf{u}_i^n = \frac{1}{\Delta s} \int_{s_{i-\frac{1}{2}}}^{s_{i+\frac{1}{2}}} \mathbf{u}(s, t^n) ds \quad \text{and} \quad \mathbf{F}_{i+\frac{1}{2}} = \frac{1}{\Delta t} \int_{t^n}^{t^{n+1}} \mathbf{F}(\mathbf{u}(s_{i+\frac{1}{2}}, t)) dt. \quad (4.14)$$

Given $\tilde{\mathbf{F}}_{i+\frac{1}{2}}$, which is an approximation of the flux $\mathbf{F}_{i+\frac{1}{2}}$, then the scheme (finite volume) to solve (4.12) is completely determined. We therefore have to compute the numerical flux $\tilde{\mathbf{F}}_{i+\frac{1}{2}}$ and we will use the ADER scheme. There are two versions of the ADER scheme which are the state-expansion and the flux expansion version. The two are identical for linear functions \mathbf{F} but differ for nonlinear \mathbf{F} . For the computation of the numerical flux we require a certain order of accuracy m . The advantage of using ADER is that it possesses a property that it can be extended to any given order of accuracy m . To compute the numerical flux we solve at each cell interface $s_{i+\frac{1}{2}}$ a general Riemann problem of degree $m - 1$ (GRP_{m-1}), but instead of

a piecewise constant initial conditions we have polynomials of degree $m - 1$ on the left and right side of the discontinuity. Thus we have to solve

$$\begin{aligned} \partial_t \mathbf{u} + \partial_s \mathbf{F}(\mathbf{u}) &= 0, \quad s \in \mathbb{R}, \quad t > t^n \\ \mathbf{u}(s, t) &= \begin{cases} \mathbf{u}_L(s) := \mathbf{p}_i(s), & s < s_{i+\frac{1}{2}} \\ \mathbf{u}_R(s) := \mathbf{p}_{i+1}(s), & s > s_{i+\frac{1}{2}} \end{cases} \end{aligned} \quad (4.15)$$

The initial conditions $\mathbf{u}_L(s)$ and $\mathbf{u}_R(s)$ are computed using some construction method described briefly later. To obtain a scheme of order m , we express the approximate solution of (GRP_{m-1}) (4.15) as a Taylor series expansion in time at the cell interface. Defining $\tau = t - t^n$, we have

$$\mathbf{u}(s_{i+\frac{1}{2}}, t) = \mathbf{u}(s_{i+\frac{1}{2}}, t^n +) + \sum_{k=1}^{m-1} \left[\partial_t^{(k)} \mathbf{u}(s_{i+\frac{1}{2}}, t^n +) \right] \frac{\tau^k}{k!} + \mathcal{O}(\tau^m), \quad (4.16)$$

where $\partial_t^k \mathbf{u}(s, t) := \frac{\partial^k}{\partial t^k} \mathbf{u}(s, t)$. The leading term $\mathbf{u}(s_{i+\frac{1}{2}}, t^n +)$ is the Godunov state solution of the conventional Riemann problem (with piecewise constant data) GRP_0

$$\begin{aligned} \partial_t \mathbf{u} + \partial_s \mathbf{F}(\mathbf{u}) &= 0, \quad s \in \mathbb{R}, \quad t > t^n \\ \mathbf{u}(s, t) &= \begin{cases} \mathbf{u}_L(s_{i+\frac{1}{2}}), & s < s_{i+\frac{1}{2}} \\ \mathbf{u}_R(s_{i+\frac{1}{2}}), & s > s_{i+\frac{1}{2}}. \end{cases} \end{aligned} \quad (4.17)$$

We now have to compute $\partial_t^{(k)} \mathbf{u}(s_{i+\frac{1}{2}}, t^n +)$ for the remaining $m - 1$ terms. Since the derivatives with respect to time are usually not available at each cell interface $s_{i+\frac{1}{2}}$, we use a method that is based on the representation of the time derivatives in terms of spatial derivatives of u ; for details see [1]. We therefore compute the spatial derivatives. We define $\mathbf{u}^{(k)} = \partial_s^{(k)} \mathbf{u}$ the k -th spatial derivative. Taking the derivative of (4.12) with respect to s we obtain

$$\begin{aligned} \mathbf{0} &= \partial_s(\partial_t \mathbf{u}) + \partial_s[\partial_s \mathbf{F}(\mathbf{u})] \\ &= \partial_t \mathbf{u}^{(1)} + \mathbf{F}'(\mathbf{u}) \partial_s \mathbf{u}^{(1)} + \partial_s(\mathbf{F}'(\mathbf{u})) \mathbf{u}^{(1)}. \end{aligned} \quad (4.18)$$

Hence, $\mathbf{u}^{(1)}$ is determined from $\partial_t \mathbf{u}^{(1)} + \mathbf{F}'(\mathbf{u}) \partial_s \mathbf{u}^{(1)} = -\partial_s (\mathbf{F}'(\mathbf{u})) \mathbf{u}^{(1)}$. Repeating the procedure of taking the derivative with respect to s of (4.12) k times, we obtain

$$\partial_t \mathbf{u}^{(k)} + \mathbf{F}'(\mathbf{u}) \partial_s \mathbf{u}^{(k)} = \mathbf{G}_k(\mathbf{u}, \mathbf{u}^{(1)}, \dots, \mathbf{u}^{(k)}). \quad (4.19)$$

The function \mathbf{G}_k is an algebraic function of \mathbf{u} and all its derivative are of degree less than or equal to k . For the linear system the function $\mathbf{G}_k = 0$. We only need $\mathbf{u}^{(k)}$ at the first instant interaction of the left and right initial states. According to [1] it is justified to neglect the source terms. The system is linearized hence we obtain the state variable $\mathbf{u}^{(k)}$ by solving the RP_0

$$\begin{aligned} \partial_t \mathbf{u}^{(k)} + \mathbf{F}'(\mathbf{u}(s_{i+\frac{1}{2}}, t^n+)) \partial_s \mathbf{u}^{(k)} &= 0, \quad s \in \mathbb{R}, \quad t > t^n \\ \mathbf{u}(s, t^n) &= \begin{cases} \mathbf{u}_L^{(k)} = \partial_s^{(k)} \mathbf{u}_L(s_{i+\frac{1}{2}}), & s < s_{i+\frac{1}{2}} \\ \mathbf{u}_R^{(k)} = \partial_s^{(k)} \mathbf{u}_R(s_{i+\frac{1}{2}}), & s > s_{i+\frac{1}{2}}. \end{cases} \end{aligned} \quad (4.20)$$

We note that, to obtain the state variables for the numerical flux we solve one nonlinear and $m - 1$ linear Riemann-problems. We express time derivatives in terms of space derivatives. After computing all spatial derivatives we set up the Taylor expansion (4.16) as follows

$$\mathbf{u}(s_{i+\frac{1}{2}}, \tau) = \mathbf{C}_0 + \mathbf{C}_1 \tau + \dots + \mathbf{C}_{m-1} \frac{\tau^{m-1}}{(m-1)!}. \quad (4.21)$$

\mathbf{C}_k are constant vectors obtained from the Cauchy-Kovalevskaya method [14] together with spatial derivatives computed from (4.20). Hence (4.21) approximates the value of \mathbf{u} at the interface $s_{i+\frac{1}{2}}$ with an order of accuracy m in time.

Finally we compute the numerical flux $\tilde{\mathbf{F}}_{i+\frac{1}{2}}$. This is where the two versions of ADER differ. For the state expansion method, the numerical flux is computed by using the approximate quadrature rules. Applying Gaussian quadrature we obtain

$$\tilde{\mathbf{F}}_{i+\frac{1}{2}} = \sum_{\alpha=0}^{K_\alpha} \mathbf{F}(\mathbf{u}(s_{i+\frac{1}{2}}, \gamma_\alpha \Delta t)) \omega_\alpha, \quad (4.22)$$

where γ_α and ω_α are properly chosen nodes and weights. K_α is the number of nodes and has to be chosen accordingly to the order m . For the flux

expansion version, we consider the Taylor series expansion of the physical flux with respect to time

$$\mathbf{F}(s_{i+\frac{1}{2}}, t) = \mathbf{F}(s_{i+\frac{1}{2}}, t^n +) \sum_{k=1}^{m-1} [\partial_t^{(k)} \mathbf{F}(s_{i+\frac{1}{2}}, t^n +)] \frac{\tau^k}{k!} + \mathcal{O}(\tau^m). \quad (4.23)$$

Hence, from (4.14) and (4.23), omitting the term $\mathcal{O}(\tau^m)$, the numerical flux is given by

$$\tilde{\mathbf{F}}_{i+\frac{1}{2}} = \mathbf{F}(s_{i+\frac{1}{2}}, t^n +) + \sum_{k=1}^{m-1} [\partial_t^{(k)} \mathbf{F}(s_{i+\frac{1}{2}}, t^n +)] \frac{\Delta t^k}{(k+1)!}. \quad (4.24)$$

The first term of (4.24) accounts for the interaction of the initial data and it is approximated using monotone flux functions like Godunov, Lax-Friedrich, etc [1]. in terms of the left and right cell boundary values. The other terms are computed by taking the derivatives of $\mathbf{F}(\mathbf{u})$ with respect to time t up to order $m - 1$. These two methods (4.22) and (4.24) are the same for a linear system since we can compute the integral (4.14) exactly.

4.3.1 ADER scheme for a linear system

In this section we apply the scheme derived in the previous section to the linear system of conservation laws (3.15). Since both the state-expansion and the flux-expansion versions of ADER give the same results for the linear system we can choose either one of the two. We will therefore use the state-expansion. To compute the numerical flux we first solve the appropriate Generalized Riemann problem GRP_{m-1} . Its solution will then be expressed in terms of a Taylor series expansion, see(4.16). We then express the time derivatives in terms of spatial derivatives $\partial_s^{(k)} \mathbf{u}(s, t)$. The first derivative $\partial_t \mathbf{u}(s, t)$ follow from the conservation law

$$\partial_t \mathbf{u}(s, t) = -\mathbf{A} \partial_s \mathbf{u}(s, t). \quad (4.25)$$

Taking the time derivative of (4.25), we obtain the second time derivative $\partial_t^{(2)} \mathbf{u}(s, t) = \mathbf{A}^2 \partial_s^{(2)} \mathbf{u}(s, t)$. Therefore, we can conclude by induction for general k , we have the $k - th$ time derivative

$$\partial_t^{(k)} \mathbf{u}(s, t) = (-\mathbf{A})^k \partial_s^{(k)} \mathbf{u}(s, t). \quad (4.26)$$

The determination of the time derivatives of \mathbf{u} reduces to the estimation of the spatial derivatives $\mathbf{u}^{(k)}(s, t)$. The spatial states $\mathbf{u}^{(k)}(s, t)$ are associated to the conventional Riemann problem RP_0

$$\begin{aligned} \partial_t \mathbf{u} + \mathbf{A} \partial_s \mathbf{u}^{(k)} &= \mathbf{0}, \quad s \in \mathbb{R}, \quad t > t^n \\ \mathbf{u}^{(k)}(s, t^n) &= \begin{cases} \mathbf{u}_L^{(k)} = \mathbf{u}_L^{(k)}(s_{i+\frac{1}{2}}), & s < s_{i+\frac{1}{2}} \\ \mathbf{u}_R^{(k)} = \mathbf{u}_R^{(k)}(s_{i+\frac{1}{2}}), & s > s_{i+\frac{1}{2}} \end{cases} \end{aligned} \quad (4.27a)$$

The sought particular values of the solutions to GRP_0 is $\mathbf{u}^{(k)}(s_{i+\frac{1}{2}}, t^n+)$, the so-called the Godunov state. Using (4.26), the Taylor expansion reads

$$\mathbf{u}(s_{i+\frac{1}{2}}, t) = \mathbf{u}(s_{i+\frac{1}{2}}, t^n+) + \sum_{k=1}^{m-1} \left[(-\mathbf{A})^k \mathbf{u}^{(k)}(s_{i+\frac{1}{2}}, t^n+) \right] \frac{\tau^k}{k!} + \mathcal{O}(\tau^m), \quad (4.28)$$

and hence the flux is computed from (4.14), i.e.,

$$\tilde{\mathbf{F}}_{i+\frac{1}{2}} = \mathbf{A} \mathbf{u}(s_{i+\frac{1}{2}}, t^n+) + \sum_{k=1}^{m-1} \left[(-\mathbf{A})^k \mathbf{u}^{(k)}(s_{i+\frac{1}{2}}, t^n+) \right] \frac{\Delta t^k}{(k+1)!}. \quad (4.29)$$

The cell average value \mathbf{u}_i^{n+1} in the next step is given by (4.13). Finally we have to compute the solutions of $GRP_0 \mathbf{u}^{(k)}(s, \tau)$. We are interested in the Godunov state $\mathbf{u}^{(k)}(s_{i+\frac{1}{2}}, t^n+)$. For the linear system (4.1) the solution can be expressed explicitly. We therefore express the solution of (4.27) in terms of eigenvectors (4.2), i.e;

$$\mathbf{u}_i^{(k)}(s, t) = \sum_{j=1}^2 \tilde{u}_{j,i}^{(k)}(s, t) \mathbf{r}_j, \quad (4.30)$$

with scalar functions $\tilde{u}_{j,i}^{(k)}(s, t)$ to be determined later. The double notation j, i is emphasized since $\tilde{u}_{j,i}^{(k)}$ differ for every i . The initial functions $\mathbf{u}_L(s)$ and $\mathbf{u}_R(s)$ can also decoupled since \mathbf{v}_1 and \mathbf{v}_2 are linearly independent. We obtain

$$\mathbf{u}_L^{(k)}(s_{i+\frac{1}{2}}) = \sum_{j=1}^2 \alpha_{j,i}^{(k)} \mathbf{v}_j \quad \text{and} \quad \mathbf{u}_R^{(k)}(s_{i+\frac{1}{2}}) = \sum_{j=1}^2 \beta_{j,i}^{(k)} \mathbf{v}_j, \quad (4.31)$$

with suitable constants $\alpha_{j,i}^{(k)}$ and $\beta_{j,i}^{(k)}$. We are now considering the decoupled system of equations. Using knowledge of the linear advection equation, the scalar function are given by

$$\begin{aligned} \tilde{u}_{j,i}^{(k)}(s - s_{i+\frac{1}{2}}, t) &= \tilde{u}_{j,i}^{(k)}(s - s_{i+\frac{1}{2}} - \lambda_j(t - t^n), t^n) \\ &= \begin{cases} \alpha_{j,i}^{(k)}, & \frac{s - s_{i+\frac{1}{2}}}{t - t^n} < \lambda_j, \\ \beta_{j,i}^{(k)}, & \frac{s - s_{i+\frac{1}{2}}}{t - t^n} > \lambda_j. \end{cases} \end{aligned} \quad (4.32)$$

The values $\tilde{u}_{j,i}^{(k)}(s_{i+\frac{1}{2}}, t^n+)$ correspond to the condition

$$\tilde{u}_{j,i}^{(k)}(s_{i+\frac{1}{2}}, t^n+) = \begin{cases} \alpha_{j,i}^{(k)}, & 0 < \lambda_j, \\ \beta_{j,i}^{(k)}, & 0 > \lambda_j. \end{cases} \quad (4.33)$$

We note that, since the first eigenvalue is negative and the second one is positive, the Godunov state using (4.32) and (4.33) is given by

$$\mathbf{u}_i^{(k)}(s_{i+\frac{1}{2}}, t^n+) = \beta_{1,i}^{(k)} \mathbf{r}_1 + \alpha_{2,i}^{(k)} \mathbf{r}_2. \quad (4.34)$$

4.3.2 Reconstruction and initial data

In this section we will show the basic issues, which are important for a numerical implementation of the ADER scheme. We will also present the structure of the conventional Riemann problems, i.e., we will state the initial data for arbitrary expansion index m . In this thesis we will concentrate on the cases $m = 2$ and $m = 3$ for the fixed stencil approximation and the ENO-reconstruction.

The initial polynomials $\mathbf{u}_L(s)$ and $\mathbf{u}_R(s)$ of the $GRP(m-1)$ are computed using the same construction methods. The technique is to construct the cell interface values of a function using given cell average values. Hence, given all cell averages \mathbf{u}_i^n at time t^n we should be able to construct the cell boundary values $\mathbf{u}_{i+\frac{1}{2}}^\pm$ with an accuracy of order m . These methods include the essentially nonoscillatory (ENO), weighted ENO (WENO) reconstructions

etc. From [2],[10], [11] or [12] we obtain for each interface two reconstructed values, $\mathbf{u}_{i+\frac{1}{2}}^+$ and $\mathbf{u}_{i+\frac{1}{2}}^-$. These are the cell boundary reconstructions at $s_{i+\frac{1}{2}}$ of \mathbf{u} when using a reconstruction stencil based on the $i - th$ cell (denoted by -) and the $i + 1 - th$ cell (denoted by +). For smooth functions these values are equal but they differ at discontinuities. We additionally get two reconstruction polynomials which provide the cell boundary values, which are of degree $m - 1$. These polynomials are used to set up the initial conditions of (4.17). The polynomial obtained by reconstruction based on the $i - th$ cell corresponds to $\mathbf{u}_L(s)$ while the one based on the $i + 1 - th$ cell corresponds to $\mathbf{u}_R(s)$.

Fixed stencil approximation uses a fixed (defined by the left shift r , which is fixed for all cells) stencil $S_r(i)$ for each cell I_i of length m . We have

$$S_r(i) = \{I_{i-r}, \dots, I_i, \dots, I_{i+m-r-1}\} \quad (4.35)$$

to determine $\mathbf{p}_i(s)$. For each cell we obtain from the reconstruction an interpolation polynomial $\mathbf{p}_{i,r}(s)$ of degree $m - 1$, which provides the cell interface values of the function u at $s_{i+\frac{1}{2}}$ and $s_{i-\frac{1}{2}}$ with an m -th order accuracy. These polynomials are used to set up the conventional Riemann problem RP_0 , which have to be solved to get the solution to the GRP_{m-1} . We then have the RP_0 for the cell interface $s_{i+\frac{1}{2}}$, arbitrary order $k = 0, \dots, m - 1$ and time t^n as

$$\begin{aligned} \partial_t \mathbf{u}^{(k)} + A \partial_s \mathbf{u}^{(k)} &= \mathbf{0}, \quad s \in \mathbb{R}, \quad t > t^n \\ \mathbf{u}^{(k)}(s, t^n) &= \begin{cases} \mathbf{u}_L^{(k)} = \mathbf{p}_{i,r}^{(k)}(s_{i+\frac{1}{2}}), & s < s_{i+\frac{1}{2}} \\ \mathbf{u}_R^{(k)} = \mathbf{p}_{i+1,r}^{(k)}(s_{i+\frac{1}{2}}), & s > s_{i+\frac{1}{2}} \end{cases} \end{aligned} \quad (4.36)$$

We now present the formulas for the initial values $\mathbf{u}_L^{(k)}$ and $\mathbf{u}_R^{(k)}$ at an arbitrary cell interface $s_{i+\frac{1}{2}}$. We note that these values differ in every time step n and therefore have to be calculated at each time step from the given approximation \mathbf{u}_i^n .

Fixed stencil approximation $m = 2$

For the fixed stencil reconstruction for the choice $r = 0$ we obtain, considering the cell interface $s_{i+\frac{1}{2}}$, the following initial values for the RP_0 :

$$\mathbf{u}(s, 0) = \begin{cases} \frac{1}{2}(\mathbf{u}_{i+1} + \mathbf{u}_i), & s < s_{i+\frac{1}{2}} \\ \frac{1}{2}(-\mathbf{u}_{i+2} + 3\mathbf{u}_{i+1}) & s > s_{i+\frac{1}{2}} \end{cases} \quad (4.37a)$$

$$\mathbf{u}^{(1)}(s, 0) = \begin{cases} \frac{1}{\Delta s}(\mathbf{u}_{i+1} - \mathbf{u}_i), & s < s_{i+\frac{1}{2}} \\ \frac{1}{\Delta s}(\mathbf{u}_{i+2} - \mathbf{u}_{i+1}) & s > s_{i+\frac{1}{2}} \end{cases} \quad (4.37b)$$

For the choice $r = 1$ we obtain, considering the cell interface $s_{i+\frac{1}{2}}$, the following initial values for the RP_0 :

$$\mathbf{u}(s, 0) = \begin{cases} \frac{1}{2}(3\mathbf{u}_i - \mathbf{u}_{i-1}), & s < s_{i+\frac{1}{2}} \\ \frac{1}{2}(\mathbf{u}_{i+1} + \mathbf{u}_i) & s > s_{i+\frac{1}{2}} \end{cases} \quad (4.38a)$$

$$\mathbf{u}^{(1)}(s, 0) = \begin{cases} \frac{1}{\Delta s}(\mathbf{u}_i - \mathbf{u}_{i-1}), & s < s_{i+\frac{1}{2}} \\ \frac{1}{\Delta s}(\mathbf{u}_{i+1} - \mathbf{u}_i) & s > s_{i+\frac{1}{2}} \end{cases} \quad (4.38b)$$

Fixed stencil Approximation $m = 3$

For the fixed stencil reconstruction for the choice $r = 0$ and $m = 3$ we obtain, considering the cell interface $s_{i+\frac{1}{2}}$, the following initial values for RP_0 :

$$\mathbf{u}(s, 0) = \begin{cases} \frac{1}{6}(-\mathbf{u}_{i+2} + 5\mathbf{u}_{i+1} + 2\mathbf{u}_i), & s < s_{i+\frac{1}{2}} \\ \frac{1}{6}(2\mathbf{u}_{i+3} - 7\mathbf{u}_{i+2} + 11\mathbf{u}_{i+1}) & s > s_{i+\frac{1}{2}} \end{cases} \quad (4.39a)$$

$$\mathbf{u}^{(1)}(s, 0) = \begin{cases} \frac{1}{\Delta s}(\mathbf{u}_{i+1} - \mathbf{u}_i), & s < s_{i+\frac{1}{2}} \\ \frac{1}{\Delta s}(-\mathbf{u}_{i+3} + 3\mathbf{u}_{i+2} - 2\mathbf{u}_{i+1}) & s > s_{i+\frac{1}{2}} \end{cases} \quad (4.39b)$$

$$\mathbf{u}^{(2)}(s, 0) = \begin{cases} \frac{1}{\Delta s^2}(\mathbf{u}_{i+2} - 2\mathbf{u}_{i+1} + \mathbf{u}_i), & s < s_{i+\frac{1}{2}} \\ \frac{1}{\Delta s^2}(\mathbf{u}_{i+3} - 2\mathbf{u}_{i+2} + \mathbf{u}_{i+1}) & s > s_{i+\frac{1}{2}}. \end{cases} \quad (4.39c)$$

Furthermore for $r = 1$ and $m = 3$ we have obtain the following initial value for the RP_0 :

$$\mathbf{u}(s, 0) = \begin{cases} \frac{1}{6}(2\mathbf{u}_{i+1} + 5\mathbf{u}_i - \mathbf{u}_{i-1}), & s < s_{i+\frac{1}{2}} \\ \frac{1}{6}(-\mathbf{u}_{i+2} + 5\mathbf{u}_{i+1} + 2\mathbf{u}_i), & s > s_{i+\frac{1}{2}} \end{cases} \quad (4.40a)$$

$$\mathbf{u}^{(1)}(s, 0) = \begin{cases} \frac{1}{\Delta s}(\mathbf{u}_{i+1} - \mathbf{u}_i), & s < s_{i+\frac{1}{2}} \\ \frac{1}{\Delta s}(\mathbf{u}_{i+1} - \mathbf{u}_i), & s > s_{i+\frac{1}{2}} \end{cases} \quad (4.40b)$$

$$\mathbf{u}^{(2)}(s, 0) = \begin{cases} \frac{1}{\Delta s^2}(\mathbf{u}_{i+1} - 2\mathbf{u}_i + \mathbf{u}_{i-1}), & s < s_{i+\frac{1}{2}} \\ \frac{1}{\Delta s^2}(\mathbf{u}_{i+2} - 2\mathbf{u}_{i+1} + \mathbf{u}_i), & s > s_{i+\frac{1}{2}} \end{cases} \quad (4.40c)$$

and for $r = 2$ and $m = 3$ we have the following initial conditions:

$$\mathbf{u}(s, 0) = \begin{cases} \frac{1}{6}(11\mathbf{u}_i - 7\mathbf{u}_{i-1} + 2\mathbf{u}_{i-2}), & s < s_{i+\frac{1}{2}} \\ \frac{1}{6}(2\mathbf{u}_{i+1} + 5\mathbf{u}_i - \mathbf{u}_{i-1}), & s > s_{i+\frac{1}{2}} \end{cases} \quad (4.41a)$$

$$\mathbf{u}^{(1)}(s, 0) = \begin{cases} \frac{1}{\Delta s}(2\mathbf{u}_i - 3\mathbf{u}_{i-1} + \mathbf{u}_{i-2}), & s < s_{i+\frac{1}{2}} \\ \frac{1}{\Delta s}(\mathbf{u}_{i+1} - \mathbf{u}_i), & s > s_{i+\frac{1}{2}} \end{cases} \quad (4.41b)$$

$$\mathbf{u}^{(2)}(s, 0) = \begin{cases} \frac{1}{\Delta s^2}(\mathbf{u}_i - 2\mathbf{u}_{i-1} + \mathbf{u}_{i-2}), & s < s_{i+\frac{1}{2}} \\ \frac{1}{\Delta s^2}(\mathbf{u}_{i+1} - 2\mathbf{u}_i + \mathbf{u}_{i-1}), & s > s_{i+\frac{1}{2}} \end{cases} \quad (4.41c)$$

ENO for $m = 2, 3$

The ENO reconstruction procedure is defined via the fixed stencil reconstruction, but instead of fixing the left shift r on each cell I_i , we choose r such that the function \mathbf{u} is the smoothest on the chosen stencil. The Newton divided differences are used to decide which r should be chosen. The idea is to start with a two point stencil, then add in each step another cell depending on the value of the Newton divided differences. The procedure is to be repeated until the m -th order stencil is obtained. In the case of $m = 2$ we can use either $r = 0$ or $r = 1$. Depending on the value of r we use either the results (4.37) or (4.38) as the initial data to solve the RP_0 at each cell interface $s_{i+\frac{1}{2}}$. For $m = 3$ we have three choices of r which are $r = 0$, $r = 1$ and $r = 2$ again depending on the value of r we use as the initial data of the RP_0 either one of (4.39), (4.40) or (4.41).

We now summarize the procedure discussed above for computing the numerical flux. Solving the appropriate GRP_{m-1}

$$\begin{aligned}\partial_t \mathbf{u} + \partial_s \mathbf{F}(\mathbf{u}) &= 0, \quad s \in \mathbb{R}, \quad t > t^n \\ \mathbf{u}(s, t) &= \begin{cases} \mathbf{u}_L(s) := \mathbf{p}_i(s), & s < s_{i+\frac{1}{2}} \\ \mathbf{u}_R(s) := \mathbf{p}_{i+1}(s), & s > s_{i+\frac{1}{2}} \end{cases}\end{aligned}$$

Algorithm 2 ADER flux

- 1: Express the approximate solution as a Taylor series expansion in time at the cell interface

$$\mathbf{u}(s_{i+\frac{1}{2}}, t) = \mathbf{u}(s_{i+\frac{1}{2}}, t^{n+}) + \sum_{k=1}^{m-1} \left[\partial_t^{(k)} \mathbf{u}(s_{i+\frac{1}{2}}, t^{n+}) \right] \frac{\tau^k}{k!} + \mathcal{O}(\tau^m).$$

- 2: Express time derivatives in terms of spatial derivatives

$$\partial_t^{(k)} \mathbf{u}(s, t) = (-\mathbf{A})^k \partial_s^{(k)} \mathbf{u}(s, t), \quad k = 1, 2, \dots, m-1.$$

- 3: Solve the conventional Riemann problem RP_0

$$\begin{aligned}\partial_t \mathbf{u}^{(k)} + \mathbf{A} \partial_s \mathbf{u}^{(k)} &= \mathbf{0}, \quad s \in \mathbb{R}, \quad t > t^n \\ \mathbf{u}^{(k)}(s, t^n) &= \begin{cases} \mathbf{u}_L^{(k)} = \mathbf{u}_L^{(k)}(s_{i+\frac{1}{2}}), & s < s_{i+\frac{1}{2}} \\ \mathbf{u}_R^{(k)} = \mathbf{u}_R^{(k)}(s_{i+\frac{1}{2}}), & s > s_{i+\frac{1}{2}} \end{cases}\end{aligned}$$

- 4: Express solutions to RP_0 using Taylor expansion

$$\mathbf{u}(s_{i+\frac{1}{2}}, t) = \mathbf{u}(s_{i+\frac{1}{2}}, t^{n+}) + \sum_{k=1}^{m-1} \left[(-\mathbf{A})^k \mathbf{u}^{(k)}(s_{i+\frac{1}{2}}, t^{n+}) \right] \frac{\tau^k}{k!} + \mathcal{O}(\tau^m).$$

- 5: Compute the flux

$$\tilde{\mathbf{F}}_{i+\frac{1}{2}} = \mathbf{A} \mathbf{u}(s_{i+\frac{1}{2}}, t^{n+}) + \sum_{k=1}^{m-1} \left[(-\mathbf{A})^k \mathbf{u}^{(k)}(s_{i+\frac{1}{2}}, t^{n+}) \right] \frac{\Delta t^k}{(k+1)!}.$$

4.3.3 Stability analysis

Investigating the stability of the ADER schemes is complicated, and becomes more complicated to analyze for higher m . Choosing the ENO/WENO reconstructions we would have to distinguish a lot of different cases, since different left-shifts r are used for different cells I_i and hence different combinations have to be investigated. Investigating the stability using the fixed stencil reconstruction for $m = 2$ and $r = 0$. Considering the linear advection equation

$$\partial_t + a\partial_s u = 0, \quad s \in \mathbb{R}, t > 0, a \in \mathbb{R}. \quad (4.42)$$

Where u is uniquely determined by (4.42) and the initial condition $u(s, 0) = u_0(s)$, $s \in \mathbb{R}$. We assume that $a > 0$ hence the result is right moving wave. This gives the stability condition

$$\gamma \leq 1, \quad (4.43)$$

where $\gamma = a\frac{\Delta t}{\Delta s}$, see [12] for full derivation. Subsequently, investigating the stability using the fixed stencil reconstruction for $m = 2$ and $r = 1$. Considering the advection equation (4.42) and assuming now that $a < 0$. We obtain the stability condition

$$-\gamma \leq 2. \quad (4.44)$$

We use the above conditions to investigate the stability of the decoupled system. Making use of the characteristic decomposition presented in this section, we choose different reconstruction methods for the two independent equations. We consider the fixed stencil approximation and for the left moving wave $r = 0$ and $r = 1$ for the right moving wave. From the stability conditions above, we obtained the CLF- condition $|\gamma| \leq 2$. Therefore, we obtain the restriction

$$\gamma = \lambda \frac{\Delta t}{\Delta s} \leq 2, \quad (4.45)$$

where λ is the maximum absolute eigenvalue of the considered problem.

4.4 Numerical boundary conditions

In this section we will discuss and derive the boundary conditions and the coupling conditions for the hyperbolic system (3.15). Our two span model has two boundaries at $j = 1$ and $j = 2N - 1$, the coupling condition at $j = N$ as show in Figure 4.2.

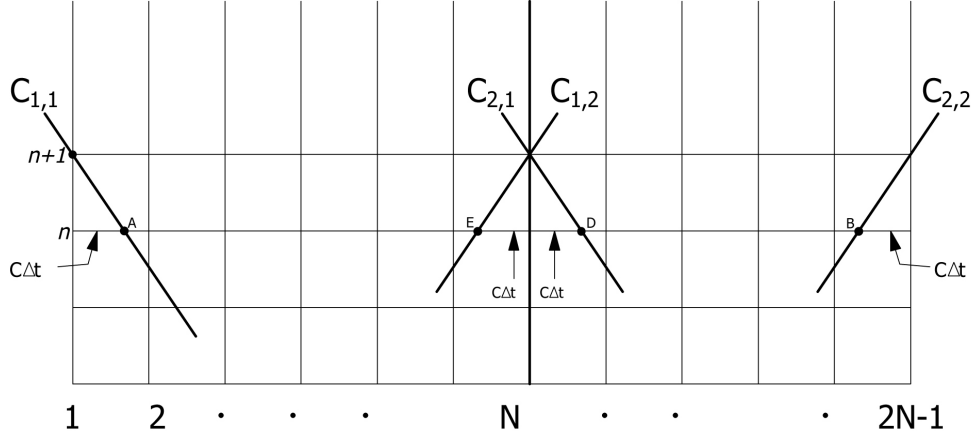


Figure 4.2: Boundary and coupling conditions of the hyperbolic system

At the left boundary, from (3.12) we have $v(0, t) = 8\mu t$ and $w(0, t)$ is unknown. We have to compute $w(0, t)$ numerically. We use the characteristic variable $\tilde{v} = R^{-1}\mathbf{v}$ and the scalar equation $\tilde{v}_t + c\tilde{v}_s = 0$. Along the first characteristic in the first span, $C_{1,1}$, we have

$$\frac{d\tilde{v}}{dt^*} = 0, \quad (4.46)$$

therefore, \tilde{v} is constant along $C_{1,1}$. We define $\tilde{v}_j^n = \tilde{v}(s_j, t^n)$, hence $\tilde{v}_1^{n+1} = \tilde{v}(A)$. We have the slope

$$\frac{ds}{dt^*} = -c = \lambda_1, \quad (4.47)$$

hence we have $s(t^*) = -c(t^* - t_{n+1}^*)$. We assume that $\gamma = c\frac{\Delta t}{\Delta s} \leq 1$. Using linear interpolation we find

$$\frac{\tilde{v}_2^n - \tilde{v}_1^n}{\Delta s} = \frac{\tilde{v}(A) - \tilde{v}_1^n}{c\Delta t}, \quad (4.48)$$

and subsequently

$$\begin{aligned} \tilde{v}(A) &= \frac{1}{\Delta s} [(\Delta s - c\Delta t)\tilde{v}_1^n + c\Delta t \tilde{v}_2^n] \\ &= (1 - \gamma)\tilde{v}_1^n + \gamma\tilde{v}_2^n. \end{aligned} \quad (4.49)$$

Since $\tilde{v}_1^{n+1} = \tilde{v}(A)$ we have

$$\tilde{v}_1^{n+1} = (1 - \gamma)\tilde{v}_1^n + \gamma\tilde{v}_2^n \quad (4.50)$$

This is just the upwind scheme for $\tilde{v}_t + c\tilde{v}_s = 0$.

From (4.4) we have

$$\tilde{v} = \frac{1}{2} \left(\frac{v}{c} + w \right) \implies w = 2\tilde{v} - \frac{v}{c}. \quad (4.51)$$

Thus we have the boundary conditions;

$$\begin{aligned} \tilde{v}_2^n &= \frac{1}{2} \left(\frac{1}{c} v_2^n + w_2^n \right), \\ v_1^{n+1} &= 8\mu t_{n+1}^*, \\ w_1^{n+1} &= 2\tilde{v}_1^{n+1} - \frac{1}{c} v_1^{n+1}. \end{aligned}$$

At the right boundary, from equation (3.12) we have $v(S_{2N-1}, t) = 8\mu t$ and $w(S_{2N-1}, t)$ has to be computed numerically. We have on $C_{2,2}$

$$\frac{ds}{dt^*} = c = \lambda_2, \quad (4.52)$$

hence we have $s(t^*) = 1 + c(t^* - t_{n+1}^*)$. Since

$$\frac{d\tilde{w}}{dt^*} = 0, \quad (4.53)$$

this means that \tilde{w} is constant along the characteristic $C_{2,2}$ hence $\tilde{w}_{2N-1}^{n+1} = \tilde{w}(B)$.

Assuming that $\gamma = c \frac{\Delta t}{\Delta s} \leq 1$, and using linear interpolation we find

$$\frac{\tilde{w}_{2N-1}^n - \tilde{w}_{2N-2}^n}{\Delta s} = \frac{\tilde{w}_{2N-1} - \tilde{w}(B)}{c\Delta t}, \quad (4.54)$$

and subsequently

$$\begin{aligned} \tilde{w}(B) &= \frac{1}{\Delta s} [c\Delta t \tilde{w}_{2N-2}^n + (\Delta s - c\Delta t) \tilde{w}_{2N-1}^n] \\ &= \gamma \tilde{w}_{2N-2}^n + (1 - \gamma) \tilde{w}_{2N-1}^n. \end{aligned} \quad (4.55)$$

Since $\tilde{w}_{2N-1}^{n+1} = \tilde{w}(B)$ we have

$$\tilde{w}_{2N-1}^{n+1} = \gamma \tilde{w}_{2N-2}^n + (1 - \gamma) \tilde{w}_{2N-1}^n. \quad (4.56)$$

From (4.4) we have

$$\tilde{w} = \frac{1}{2} \left[\frac{-v}{c} + w \right] \implies w = 2\tilde{w} + \frac{v}{c}. \quad (4.57)$$

Thus, we have

$$\begin{aligned} \tilde{w}_{2N-1}^n &= \frac{1}{2} \left(-\frac{1}{c} v_{2N-1}^n + w_{2N-1}^n \right), \\ v_{2N-1}^{n+1} &= 8\mu t_{n+1}^*, \\ w_{2N-1}^{n+1} &= 2\tilde{w}_{2N-1}^{n+1} + \frac{1}{c} v_{2N-1}^{n+1}. \end{aligned}$$

We now consider the coupling condition occurring at $j = N$. We have from (3.12) that $v(1, t^*, 1) = v(0, t^*, 2) = 8\mu t^*$. Along the characteristic $C_{1,2}$ we have

$$\frac{ds}{dt^*} = c \implies s(t^*) = 1 + c(t^* - t_{n+1}^*). \quad (4.58)$$

Since $\frac{d\tilde{w}}{dt} = 0$, it implies that \tilde{w} is constant along the characteristic $C_{1,2}$. Therefore $\tilde{w}_N^{n+1} = \tilde{w}(E)$. Assuming that $\gamma = \frac{c\Delta t}{\Delta s} < 1$ and using interpolation we obtain

$$\tilde{w}(E) = \gamma \tilde{w}_{N-1}^n + (1 - \gamma) \tilde{w}_N^n. \quad (4.59)$$

Hence we have

$$\tilde{w}_N^{n+1} = \gamma \tilde{w}_{N-1}^n + (1 - \gamma) \tilde{w}_N^n. \quad (4.60)$$

Thus;

$$\begin{aligned} \tilde{w}_N^n &= \frac{1}{2} \left(-\frac{1}{c} v_N^n + w_N^n \right), \\ v_N^{n+1} &= 8\mu t_{n+1}^*, \\ w_N^{n+1} &= 2\tilde{w}_N^{n+1} + \frac{1}{c} v_N^{n+1}. \end{aligned}$$

Similarly along $C_{2,1}$, we have

$$\frac{ds}{dt^*} = -c \implies s(t^*) = -c(t^* - t_{n+1}^*). \quad (4.61)$$

Since $\frac{d\tilde{v}}{dt} = 0$, it implies that \tilde{v} is constant along $C_{2,1}$. Therefore $\tilde{v}_N^{n+1} = \tilde{v}(D)$. Assuming that $\gamma = \frac{c\Delta t}{\Delta s} < 1$ and using interpolation we obtain

$$\tilde{v}(D) = (1 - \gamma) \tilde{v}_N^n + \gamma \tilde{v}_{N+1}^n. \quad (4.62)$$

Thus;

$$\begin{aligned}\tilde{v}_N^n &= \frac{1}{2} \left(\frac{1}{c} v_N^n + w_N^n \right). \\ v_N^{n+1} &= 8\mu t_{n+1}^*. \\ w_N^{n+1} &= 2\tilde{v}_N^{n+1} - \frac{1}{c} v_N^{n+1}.\end{aligned}$$

Chapter 5

Numerical Results

In this chapter, we illustrate the performance of the schemes presented in this thesis. We will first present numerical results and analysis of the accuracy of the ADER scheme for solving the hyperbolic system (3.15). Next we will present the simulation results of galloping transmission lines for the upwind scheme.

5.1 Numerical experiments for ADER scheme

In this section we perform numerical tests and measure the error with respect to the given analytical solution (4.5). We are expecting an error of the order m for constant CLF number, which is defined by

$$\gamma = c \frac{\Delta t}{\Delta s},$$

For our experiments we choose $T^* = 4$, therefore we get $c = 2$. Thus, the ratio between the step size Δt and the grid size Δs has to be a constant in order to obtain the desired order of accuracy m . The linear stability condition, mentioned in [1], is the CLF condition $\gamma \leq 1$. All tests are performed using the initial condition,

$$\mathbf{u}_0(s) = \begin{pmatrix} \sin \pi s \\ \cos \pi s \end{pmatrix}.$$

5.1. NUMERICAL EXPERIMENTS FOR ADER SCHEME 36

Furthermore the errors are measured in the L_∞ -norm and the L_2 -norm. The L_∞ -norm is used additionally to get an impression of the maximum error. Both errors are presented in the Tables 5.1-5.7. In each cell the upper value is the L_∞ - error and the lower is the L_2 - error. We have chosen several values for the spatial grid size and time step size for testing the order of accuracy. The final time we used to measure the error is $t_{max} = 2$ for all experiments.

Δs	Δt			
	0.08	0.04	0.02	0.01
0.2	$8.117 \cdot 10^{-2}$	$1.380 \cdot 10^{-1}$	$1.613 \cdot 10^{-1}$	$1.955 \cdot 10^{-1}$
	$7.862 \cdot 10^{-2}$	$1.337 \cdot 10^{-1}$	$1.470 \cdot 10^{-1}$	$1.387 \cdot 10^{-1}$
0.1	$6.961 \cdot 10^{10}$	$2.758 \cdot 10^{-2}$	$6.627 \cdot 10^{-2}$	$9.294 \cdot 10^{-2}$
	$3.298 \cdot 10^{10}$	$2.728 \cdot 10^{-2}$	$6.147 \cdot 10^{-2}$	$8.058 \cdot 10^{-2}$
0.05	$3.422 \cdot 10^{26}$	$2.747 \cdot 10^{24}$	$6.756 \cdot 10^{-3}$	$1.738 \cdot 10^{-2}$
	$2.128 \cdot 10^{26}$	$2.255 \cdot 10^{24}$	$7.412 \cdot 10^{-3}$	$1.758 \cdot 10^{-2}$
0.025	$1.793 \cdot 10^{41}$	$2.449 \cdot 10^{57}$	$7.311 \cdot 10^{53}$	$1.664 \cdot 10^{-3}$
	$6.709 \cdot 10^{40}$	$1.358 \cdot 10^{57}$	$5.104 \cdot 10^{53}$	$1.913 \cdot 10^{-3}$

Table 5.1: Reconstruction using the fixed stencil approximation of order $m = 2$ and left shift $r = 0$.

Δs	Δt			
	0.08	0.04	0.02	0.01
0.2	$2.047 \cdot 10^{-1}$	$3.626 \cdot 10^{-1}$	$4.183 \cdot 10^{-1}$	$4.175 \cdot 10^{-1}$
	$1.516 \cdot 10^{-1}$	$2.294 \cdot 10^{-1}$	$2.760 \cdot 10^{-1}$	$3.126 \cdot 10^{-1}$
0.1	$5.142 \cdot 10^{11}$	$5.236 \cdot 10^{-2}$	$8.592 \cdot 10^{-2}$	$1.054 \cdot 10^{-1}$
	$4.241 \cdot 10^{11}$	$4.819 \cdot 10^{-2}$	$7.349 \cdot 10^{-2}$	$9.085 \cdot 10^{-2}$
0.05	$5.858 \cdot 10^{27}$	$8.203 \cdot 10^{25}$	$1.340 \cdot 10^{-2}$	$1.875 \cdot 10^{-2}$
	$3.353 \cdot 10^{27}$	$5.907 \cdot 10^{25}$	$1.299 \cdot 10^{-2}$	$1.949 \cdot 10^{-2}$
0.025	$2.335 \cdot 10^{42}$	$6.666 \cdot 10^{58}$	$3.168 \cdot 10^{55}$	$3.397 \cdot 10^{-3}$
	$9.097 \cdot 10^{41}$	$3.302 \cdot 10^{58}$	$1.934 \cdot 10^{55}$	$3.363 \cdot 10^{-3}$

Table 5.2: Reconstruction using the fixed stencil approximation of order $m = 2$ and left shift $r = 1$.

Δs	Δt			
	0.08	0.04	0.02	0.01
0.2	$2.115 \cdot 10^{-2}$	$6.578 \cdot 10^{-1}$	$1.925 \cdot 10^1$	$1.084 \cdot 10^1$
	$1.605 \cdot 10^{-2}$	$3.420 \cdot 10^{-1}$	$9.826 \cdot 10^0$	$5.530 \cdot 10^1$
0.1	$1.268 \cdot 10^{16}$	$5.167 \cdot 10^{-3}$	$1.733 \cdot 10^0$	$3.181 \cdot 10^4$
	$1.118 \cdot 10^{16}$	$3.978 \cdot 10^{-3}$	$8.672 \cdot 10^{-1}$	$1.153 \cdot 10^4$
0.05	$1.754 \cdot 10^{38}$	$2.683 \cdot 10^{36}$	$9.059 \cdot 10^{-4}$	$5.157 \cdot 10^3$
	$1.139 \cdot 10^{38}$	$2.131 \cdot 10^{36}$	$6.916 \cdot 10^{-4}$	$2.567 \cdot 10^3$
0.025	$6.645 \cdot 10^{58}$	$1.267 \cdot 10^{81}$	$3.326 \cdot 10^{78}$	$1.233 \cdot 10^{-4}$
	$3.105 \cdot 10^{58}$	$7.162 \cdot 10^{88}$	$2.541 \cdot 10^{78}$	$1.009 \cdot 10^{-4}$

Table 5.3: Reconstruction using the fixed stencil approximation of order $m = 3$ and left shift $r = 0$.

Δs	Δt			
	0.08	0.04	0.02	0.01
0.2	$1.957 \cdot 10^{-2}$	$2.006 \cdot 10^{-2}$	$2.032 \cdot 10^{-2}$	$2.292 \cdot 10^{-2}$
	$1.577 \cdot 10^{-2}$	$1.715 \cdot 10^{-2}$	$1.831 \cdot 10^{-2}$	$1.912 \cdot 10^{-2}$
0.1	$3.700 \cdot 10^{-3}$	$3.100 \cdot 10^{-3}$	$5.591 \cdot 10^{-3}$	$7.136 \cdot 10^{-3}$
	$3.381 \cdot 10^{-3}$	$3.266 \cdot 10^{-3}$	$4.840 \cdot 10^{-3}$	$5.695 \cdot 10^{-3}$
0.05	$3.208 \cdot 10^{26}$	$7.471 \cdot 10^{-4}$	$6.857 \cdot 10^{-4}$	$1.715 \cdot 10^{-3}$
	$2.858 \cdot 10^{26}$	$6.030 \cdot 10^{-4}$	$5.229 \cdot 10^{-4}$	$1.026 \cdot 10^{-3}$
0.025	$3.497 \cdot 10^{53}$	$6.424 \cdot 10^{57}$	$1.128 \cdot 10^{-4}$	$1.023 \cdot 10^{-4}$
	$2.341 \cdot 10^{53}$	$4.228 \cdot 10^{57}$	$8.826 \cdot 10^{-5}$	$7.339 \cdot 10^{-5}$

Table 5.4: Reconstruction using the fixed stencil approximation of order $m = 3$ and left shift $r = 1$.

In the Tables 5.1 and 5.2 the errors of the fixed stencil approximation for $m = 2$ are depicted. The Tables 5.3-5.5 show the errors of the fixed stencil approximation for $m = 3$. The errors for the ENO reconstruction for $m = 2$ and $m = 3$ are shown in Tables 5.6 and 5.7 respectively. On the diagonal of the tables the *CLF* condition number γ has the value 0.8. We note that on the lower subdiagonal the methods are unstable since $\gamma > 1$ there. Table 5.8 presents the L_2 - and L_∞ - error orders for several grid sizes Δs and the constant CLF-number $\gamma = 0.8$.

From 5.8 we see that we achieve the desired order of accuracy using the fixed point approximation when compared to ENO. We note that in our case we are only considering continuous function, if we would consider the discontinuous

Δs	Δt			
	0.08	0.04	0.02	0.01
0.2	$6.754 \cdot 10^{-2}$	$1.694 \cdot 10^0$	$5.076 \cdot 10^1$	$2.856 \cdot 10^2$
	$4.841 \cdot 10^{-2}$	$8.611 \cdot 10^{-1}$	$2.710 \cdot 10^1$	$1.526 \cdot 10^2$
0.1	$6.094 \cdot 10^{16}$	$1.302 \cdot 10^{-2}$	$5.304 \cdot 10^0$	$8.341 \cdot 10^4$
	$5.374 \cdot 10^{16}$	$1.005 \cdot 10^{-2}$	$2.818 \cdot 10^0$	$3.449 \cdot 10^4$
0.05	$8.341 \cdot 10^4$	$1.305 \cdot 10^{37}$	$2.783 \cdot 10^{-3}$	$1.151 \cdot 10^4$
	$3.449 \cdot 10^4$	$1.039 \cdot 10^{37}$	$1.514 \cdot 10^{-3}$	$5.902 \cdot 10^3$
0.025	$3.2083 \cdot 10^{59}$	$6.260 \cdot 10^{81}$	$1.639 \cdot 10^{79}$	$3.895 \cdot 10^{-4}$
	$1.522 \cdot 10^{59}$	$3.547 \cdot 10^{81}$	$1.255 \cdot 10^{79}$	$2.032 \cdot 10^{-4}$

Table 5.5: Reconstruction using the fixed stencil approximation of order $m = 3$ and left shift $r = 2$.

Δs	Δt			
	0.08	0.04	0.02	0.01
0.2	$1.265 \cdot 10^{-1}$	$1.704 \cdot 10^{-1}$	$1.814 \cdot 10^{-1}$	$1.929 \cdot 10^{-1}$
	$1.208 \cdot 10^{-1}$	$1.345 \cdot 10^{-1}$	$1.470 \cdot 10^{-1}$	$1.399 \cdot 10^{-1}$
0.1	$2.469 \cdot 10^5$	$3.197 \cdot 10^{-2}$	$9.260 \cdot 10^{-2}$	$1.655 \cdot 10^{-1}$
	$1.521 \cdot 10^5$	$3.415 \cdot 10^{-2}$	$6.216 \cdot 10^{-2}$	$9.571 \cdot 10^{-2}$
0.05	$6.404 \cdot 10^{18}$	$1.185 \cdot 10^{14}$	$7.703 \cdot 10^{-3}$	$2.597 \cdot 10^{-2}$
	$2.929 \cdot 10^{18}$	$4.839 \cdot 10^{13}$	$8.899 \cdot 10^{-3}$	$1.361 \cdot 10^{-2}$
0.025	$1.843 \cdot 10^{32}$	$5.094 \cdot 10^{40}$	$5.188 \cdot 10^{29}$	$2.062 \cdot 10^{-3}$
	$8.653 \cdot 10^{31}$	$1.606 \cdot 10^{40}$	$1.620 \cdot 10^{29}$	$2.287 \cdot 10^{-3}$

Table 5.6: Reconstruction using the ENO of order $m = 2$.

solution, the fixed stencil approximation would lead to oscillations. The performance of ENO could have been affected due to numerical flux not being continuous.

Δs	Δt			
	0.08	0.04	0.02	0.01
0.2	$1.957 \cdot 10^{-2}$	$2.006 \cdot 10^{-2}$	$2.032 \cdot 10^{-2}$	$2.282 \cdot 10^{-2}$
	$1.577 \cdot 10^{-2}$	$1.715 \cdot 10^{-2}$	$1.830 \cdot 10^{-2}$	$1.909 \cdot 10^{-2}$
0.1	$8.320 \cdot 10^3$	$3.115 \cdot 10^{-3}$	$6.004 \cdot 10^{-3}$	$8.865 \cdot 10^{-3}$
	$2.711 \cdot 10^3$	$3.290 \cdot 10^{-3}$	$5.199 \cdot 10^{-3}$	$6.947 \cdot 10^{-3}$
0.05	$3.032 \cdot 10^{26}$	$2.481 \cdot 10^{12}$	$6.858 \cdot 10^{-4}$	$1.713 \cdot 10^{-3}$
	$9.108 \cdot 10^{25}$	$7.222 \cdot 10^{11}$	$5.229 \cdot 10^{-4}$	$1.028 \cdot 10^{-3}$
0.025	$2.009 \cdot 10^{47}$	$3.352 \cdot 10^{57}$	$3.009 \cdot 10^{32}$	$1.021 \cdot 10^{-4}$
	$6.739 \cdot 10^{46}$	$1.367 \cdot 10^{57}$	$5.443 \cdot 10^{31}$	$7.335 \cdot 10^{-5}$

Table 5.7: Reconstruction using the ENO of order $m = 3$.

ADER scheme	Δs	Δt	L_2 error	L_2 order	L_∞ error	L_∞ order
$m = 2$	0.2	0.08	$1.516 \cdot 10^{-1}$		$2.047 \cdot 10^{-1}$	
FSA	0.1	0.04	$4.819 \cdot 10^{-2}$	1.87	$5.236 \cdot 10^{-2}$	1.95
$r = 1$	0.05	0.02	$1.299 \cdot 10^{-2}$	1.85	$1.311 \cdot 10^{-2}$	1.95
	0.025	0.01	$3.363 \cdot 10^{-3}$	1.93	$3.397 \cdot 10^{-3}$	2.00
$m = 3$	0.2	0.08	$1.577 \cdot 10^{-2}$		$1.957 \cdot 10^{-2}$	
FSA	0.1	0.04	$3.266 \cdot 10^{-3}$	2.41	$3.100 \cdot 10^{-3}$	3.16
$r = 1$	0.05	0.02	$5.229 \cdot 10^{-4}$	3.12	$6.857 \cdot 10^{-4}$	3.26
	0.025	0.01	$7.339 \cdot 10^{-5}$	3.56	$1.023 \cdot 10^{-4}$	3.35
$m = 2$	0.2	0.08	$1.208 \cdot 10^{-1}$		$1.265 \cdot 10^{-1}$	
ENO	0.1	0.04	$3.415 \cdot 10^{-2}$	1.77	$3.197 \cdot 10^{-2}$	1.98
	0.05	0.02	$8.899 \cdot 10^{-3}$	1.92	$7.703 \cdot 10^{-3}$	2.08
	0.025	0.01	$2.287 \cdot 10^{-3}$	1.94	$2.062 \cdot 10^{-3}$	1.87
$m = 3$	0.2	0.08	$1.577 \cdot 10^{-2}$		$1.957 \cdot 10^{-2}$	
ENO	0.1	0.04	$3.290 \cdot 10^{-3}$	2.40	$3.115 \cdot 10^{-3}$	3.14
	0.05	0.02	$5.229 \cdot 10^{-4}$	3.15	$6.858 \cdot 10^{-4}$	2.27
	0.025	0.01	$7.335 \cdot 10^{-5}$	3.56	$1.021 \cdot 10^{-4}$	3.39

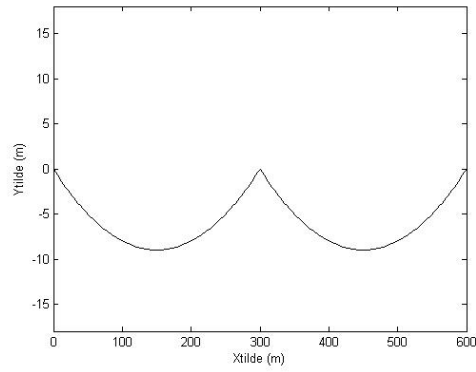
Table 5.8: L_2 and L_∞ errors and orders for different Δs , $\gamma = 0.8$ and $tmax = 2$.

5.2 Cable simulation results

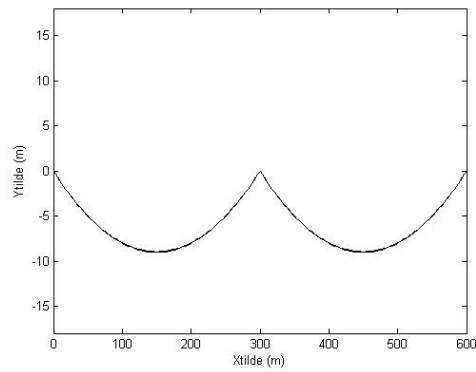
We now show examples of a two span model simulation. The parameters used are practically relevant and were taken from [3]. In all cases we have used $m = 1 \text{ kg/m}$, $g = 9.8 \text{ m/s}^2$, $EA = 2.156 \times 10^7 \text{ N}$, $S = 320 \text{ m}$, $D = 9 \text{ m}$

and time step $\Delta t = 10^{-3}$ for grid sizes $\Delta s = 0.01$ and initial positions of the cable. The final time used is $t_{max} = 10$. For all the experiments the upwind scheme was used.

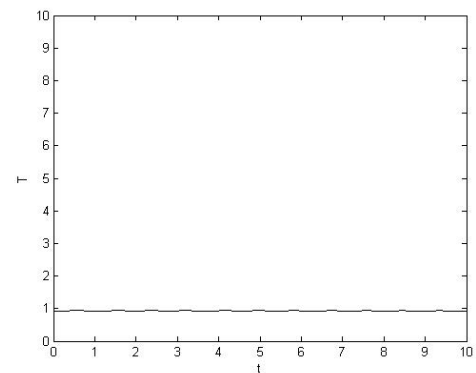
In the first simulation, we present the initial the position of the cable, that is the steady state of the cable. We then multiply the the initial conditions of the steady solution by several factors to change the initial position of the cable for simulations. The results below show the initial position of the cable, the vertical displacement of the cable and the tension against time in each simulation.



(a) Initial position of the cable

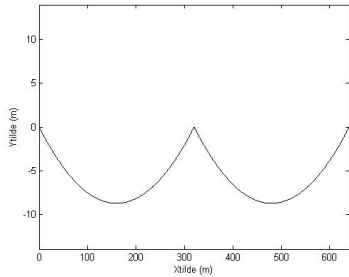


(b) Vertical displacement of the cable

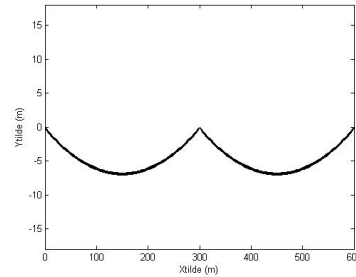


(c) Tension against time

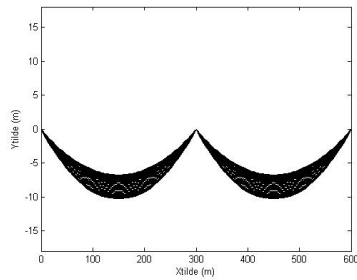
Figure 5.1: An oscillating cable section, for $N_s=100$ and has minimum at $D = 9m$ in both spans, the steady state solution.



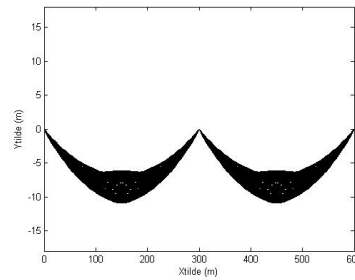
(a) Initial position of the cable



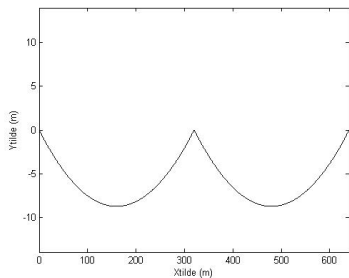
(b) Displacement of the cable at $t = 0.1$



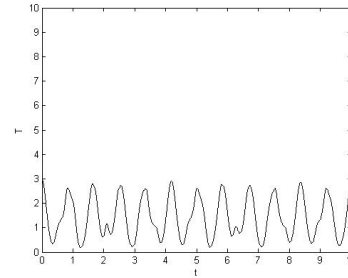
(c) Displacement of the cable at $t = 0.4$



(d) Displacement of the cable at $t = 1$

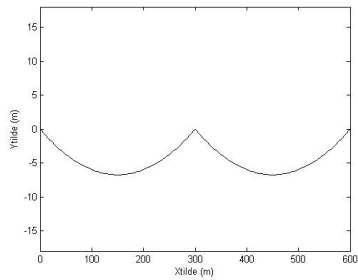


(e) Displacement of the cable at $t = 10$

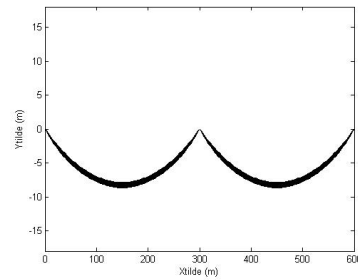
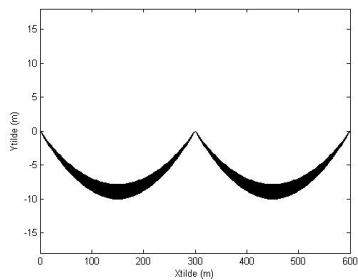
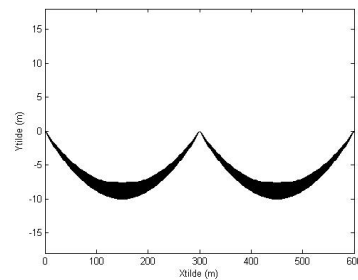
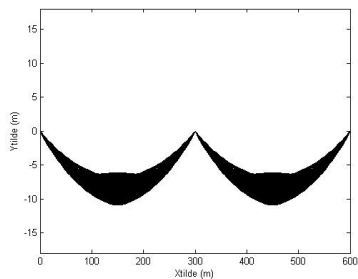
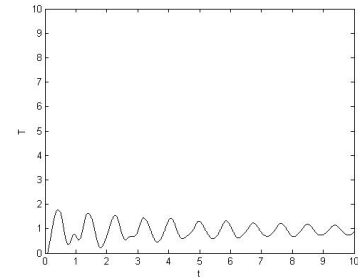


(f) Tension against time

Figure 5.2: An oscillating cable section, for $N_s=100$ and has a minimum=
at $8m$.

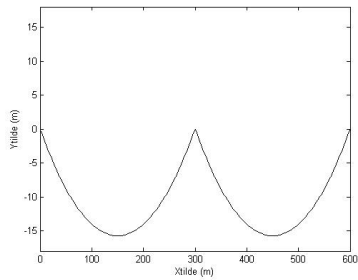


(a) Initial position of the cable

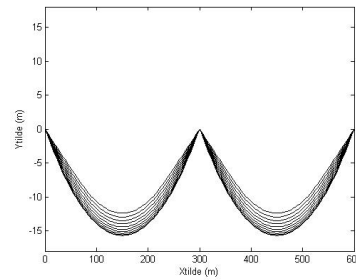
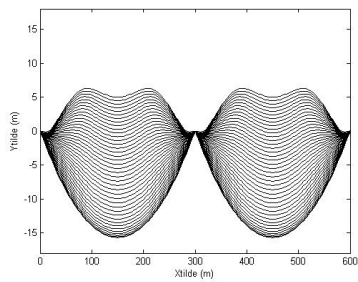
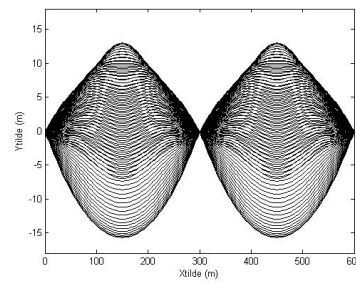
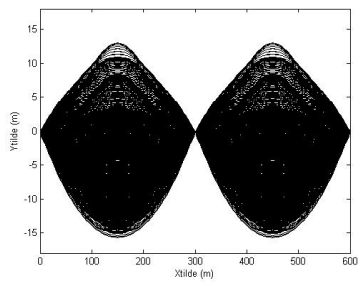
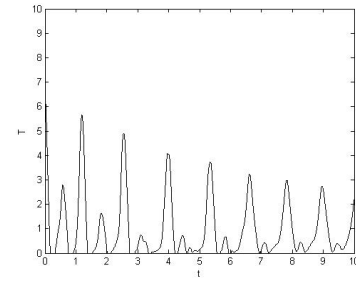
(b) Vertical displacement of the cable at $t = 0.2$ (c) Vertical displacement of the cable at $t = 0.7$ (d) Vertical displacement of the cable at $t = 1.2$ (e) Vertical displacement of the cable at $t = 10$ 

(f) Tension against time

Figure 5.3: An oscillating cable section, for $N_s=100$ and initially has a minimum at $6m$ in both spans.

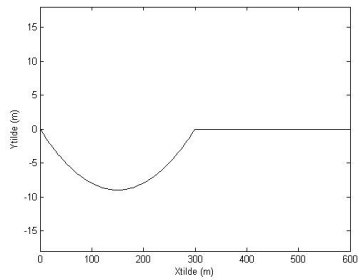


(a) Initial position of the cable

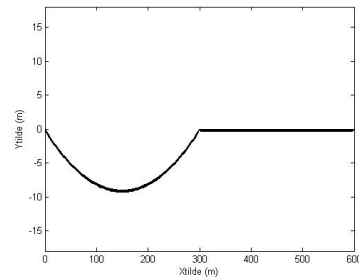
(b) Vertical displacement of the cable at $t = 0.1$ (c) Vertical displacement of the cable at $t = 0.4$ (d) Vertical displacement of the cable at $t = 1$ (e) Vertical displacement of the cable at $t = 10$ 

(f) Tension against time

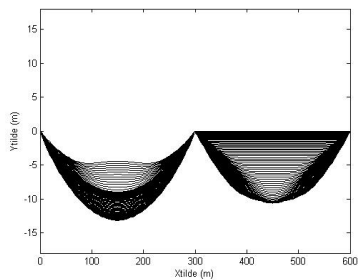
Figure 5.4: An oscillating cable section, for $N_s=100$ and has a minimum at $15m$ in both spans.



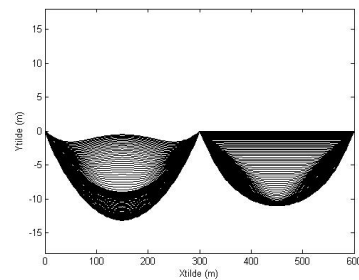
(a) Initial position of the cable



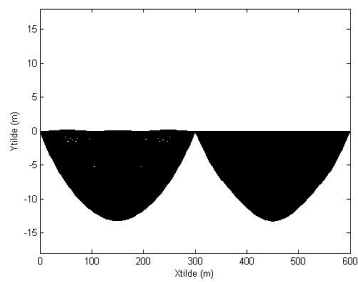
(b) Vertical displacement of the cable at $t = 0.1$



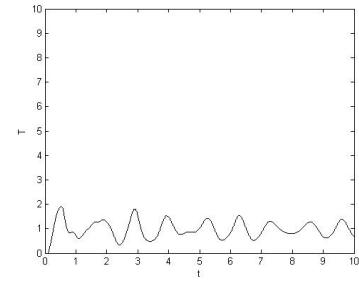
(c) Vertical displacement of the cable at $t = 0.8$



(d) Vertical displacement of the cable at $t = 1$



(e) Vertical displacement of the cable at $t = 10$



(f) Tension against time

Figure 5.5: An oscillating cable section, for $N_s=100$ and has minimum at $9m$ in the first span and 0 in the second span.

The first case Figure 5.1, we have a steady solution. Tension is constant throughout, this is expected because the cable is stationary. In the second case, the initial conditions of a steady state are changed such that the cable is raised up such that it has a minimum at $8m$. When released the cable falls down first and oscillate up and down. The results are shown in Figure 5.2. In the first subfigure the initial position of the cable is shown, the next one shows the vertical displacement of the cable as it oscillates and the last figure shows tension variation in time. For the third case we repeat the same procedure but with the minimum is at $6m$ and for the fourth case the minimum is at $15m$. In last case we change the initial position only on the second span such that minimum of the cable in the second span is at 0 . When released, on the second span the cable falls down and the motion is transferred to the first span. This is expected as we have middle point is not fixed, we have coupling conditions.

The motion of the cable seems to be symmetric for the first four tests, but that's not the case for the last test. The last test clearly shows the decoupling galloping as the motion is transferred from span to another. The tension is changing per unit time when the cable vibrates, this is expected because as the cable displacement changes the tension is also affected. From analysis of the system we expect tension to be greater than zero, and this is the case with our results. The length of the cable, L , does not change throughout the computation.

Chapter 6

Conclusion and Recommendations

The problem of galloping transmission lines was simulated. The model was first derived from first principles of Newton's and Hooke's laws. Asymptotic analysis was used to reduce the problem, by exploiting the geometrical thickness and relative elasticity, resulting in a system of equations to be solved numerically. Practically relevant parameter were used to simulate the motion of the cable in Matlab. Two schemes, the upwind and ADER, were implemented. Although the ADER schemes showed more accurate and stable results when solving linear hyperbolic conservation laws, it is complicated to implement the scheme to solve the system. This could be due to the fact that the tension is changing per time step, hence the matrix is not fixed. Therefore several tests were conducted using the upwind scheme. The motion is symmetric when the same initial conditions are set on both spans. For the case where different initial conditions were set per span, the motion was seen to be asymmetric then tends to be symmetric after some time.

The results we obtained do not clarify the characteristics of the galloping phenomenon, which could be used to prevent galloping. Therefore the following are possible suggestions for the extension of the work.

- Propose various external driving forces that improve the model.
- Derive ADER schemes for a non-fixed matrix
- Formulate and simulate the related problem for motion of the cable in three dimensions.

- Conduct several galloping simulations under various analytical conditions.

Bibliography

- [1] E. F. Toro and V.A. Titarev, *TVD Fluxes for the High-Order ADER Schemes*, Journal of Scientific Computing, **24** (2005), no. 3, 285–309.
- [2] B. Cockburn, C. Johnson, C.W. Shu, and E.Tadmor, *Advanced Numerical Approximation of Nonlinear Hyperbolic Equations.*, Lecture Notes in Mathematics, Springer, Italy, **5(4)** (1997), 325434.
- [3] Sjoerd W. Rienstra, *Nonlinear Free Vibration of Coupled Spans of Overhead Transmission Lines*, Proceedings of the Third European Conference on Mathematics in Industry **27-31** (1988), 133–144.
- [4] R.M.M Mattheij, S.W Rienstra and J.H.M ten Boonkamp, *Partial Differential Equations : Modelling, Analysis, Computation*, Philadelphia : SIAM, (2005).
- [5] J. H. Zhang, Y. H. Shi and G. X. Liu., *Simulation of Transmission Line Galloping Using Finite Element Method* IEE 2nd International Conference on Advances in Power System Control, Operation and Management, Hong Kong 1993, 644–648.
- [6] C.M Bender and S.A Orszag , *Advanced Mathematical Methods for Scientists and Engineers* , New York : McGraw Hill, (1978).
- [7] H.M. Irvine and T.K. Caughey , *The Linear Theory of Free Vibrations of a Suspended Cable*, Proceedings of the Royal Society of London. Series A, Mathematical and Physical Sciences.**341** (1974), 299–315.
- [8] Public Service Commission of Wisconsin, *Electric transmission lines: Electricity From Power Plants to Consumers.* URL: <http://psc.wi.gov/thelibrary/publications/electric/electric09.pdf>
- [9] L.D. Landau and E.M Lifshitz, *Theory of Elasticity*, Oxford: Pergamon Press, (1970).

-
- [10] C. W. Shu and S. Osher, *Efficient implementation of essential non-oscillatory shock capturing schemes*, Journal of Computational Physics, **77** (1988), 439–471.
- [11] G.S. Jiang and C. W. Shu , *Efficient implementation of Weighted ENO Schemes*, Journal of Computational Physics, **126** (1996), 202–228.
- [12] Erwin Karer, *Higher Order ADER Schemes for Linear Hyperbolic systems*, Capita Selecta report, Technische Universiteit Eindhoven, (2006).
- [13] E.F Toro, *Derivative Riemann solvers for Systems of conservation Laws and ADER Methods*, Laboratory of Applied Mathematics, Faculty of engineering, University of Trento, Italy.
- [14] M. Renardy S.W and R.C. Rogers, *An introduction to Partial Differential Equations*, Texts in Applied Mathematics, Series 13, Second Edition, Springer , (2003).
- [15] D. Gottlieb, M. Gunzburger and E. Turkel , *On Numerical Boundary Treatment of Hyperbolic Systems for Finite Difference and Finite Element Methods*, SIAM Journal on Numeric Analysis, **19** (1982), 671–682.